Collapse behaviour of a fire engineering designed single-storey cold- formed steel building in severe fires

Roy, Krishanu; Lim, James B.P.; Lau, Hieng Ho; Yong, P.M.; Clifton, G.C.; Wrzesien, Andrzej; Mei, Chee Chiang

Published in:
Thin-Walled Structures

DOI:
10.1016/j.tws.2019.04.046

Published: 30/09/2019

Document Version
Peer reviewed version

Collapse behaviour of a fire engineering designed single-storey cold- formed steel building in severe fires

Roy, Krishanu; Lim, James B.P.; Lau, Hieng Ho; Yong, P. M.; Clifton, G. C.; Wrzesien, Andrzej; Mei, Chee Chiang

Published in:
Thin-Walled Structures

DOI:
10.1016/j.tws.2019.04.046

Published: 01/09/2019

Collapse Behaviour of a Fire Engineering Designed Single-Storey Cold-Formed Steel Building in Severe Fires

Krishanu Roy [a*], James B.P. Lim [a], Hieng Ho Lau [b] P.M Yong [c], G. C. Clifton [a],

Ross P.D. Johnston [d], Andrzej Wrzesien [e], Chee Chiang Mei [f]

[a] Department of Civil and Environmental Engineering, The University of Auckland, New Zealand

[b] Faculty of Engineering, Computing and Science, Swinburne University of Technology, Sarawak Campus, Kuching, Sarawak, Malaysia

[c] Faculty of Engineering and Science, Curtin University, Miri, Malaysia

[d] Hanna and Hutchinson Consulting Engineers Ltd, Wallace Avenue, Lisburn, Northern Ireland

[e] CEPS, University of the West of Scotland, Paisley, High Street, PA1 2BE, United Kingdom

[f] Eco Steel Sdn Bhd, Kuching, Sarawak, Malaysia

[*]Corresponding Author Contact Details:

Krishanu Roy

E: kroy405@aucklanduni.ac.nz, Building 906, Level 4, Room 413, Newmarket campus, The University of Auckland, Auckland-1023, New Zealand T: +64 223917991 , F: +64 9 373 7462

Abstract:

This paper describes a full-scale natural fire test to investigate the collapse behaviour of a single storey cold-formed steel (CFS) building, designed to behave in a specified way in a severe fire, with roof venting and partial wall collapse. The test building had a span of 8 m, height-to-eaves of 2.15 m, and length of 10 m. The walls of the CFS building were constructed from cantilever 'stud & track' panels, with stud spacing of 0.6 m. The roof of the building comprised CFS trusses pinned to the wall connection plates at the top. In this fire test, walls on two adjacent sides were lined internally with fire resistant lining to achieve a structural fire resistance of 30 minutes (R30) and the calculated fire load was provided to generate a structural fire severity of 30 minutes, taking into account roof venting. Thus the two protected walls were expected to

remain vertical throughout the fire; the roof was expected to collapse first, followed by pulling in of the unprotected walls. The CFS cantilever wall / roof truss system collapsed with an inwards asymmetrical collapse mechanism at a truss temperature of 622.5 °C, with collapse being due to member buckling of the non-fire rated wall rather than failure of the screws or joints. A non-linear finite-element (FE) model is then described. The collapse temperature predicted using the FE was 628.2 °C, with a deformed shape similar to that observed in the fire test. The FE model has matched the experimental behaviour, thus making this model useful in understanding and predicting the behaviour of CFS cantilever wall / truss system in severe fire conditions.

Keywords: Cold-formed steel; Cantilever wall / roof truss system; Fire; Finite element model; Full scale test; Structural fire engineering.

Notations

CFS	Cold-formed steel;
E	Young's modulus of elasticity;
h	Thermal convection coefficient;
I_{xx}	Moment of inertia about major axis;
I_{yy}	Moment of inertia about minor axis;
L	Length of the lip of channel section;
r	Radiation emissivity;
R	Thermal radius constant;
T	Surface temperature;
T_0	Absolute zero temperature;
ε	Engineering strain;
$\varepsilon_{true,p}$	True plastic strain;
σ	Engineering stress;
σ_{true}	True stress;
σ_Z	Stefan Boltzmann constant;

1 Introduction

Single storey cold-formed steel (CFS) buildings are a popular form of construction in Malaysia and South East Asia, where they are used for low-rise residential and light industrial construction. The walls of these cold-formed steel buildings are normally constructed from cantilever 'stud & track' panels and the roof of the building comprises cold-formed steel trusses pinned to the wall connection plates at the top (see Fig. 1). This form of construction will be referred to as a cantilever wall/truss system throughout this paper. Some of the advantages of cold-formed steel cantilever wall/truss system are: light weight, ease and precision in fabrication, speed of construction, non-combustibility and resistance to insect infestation.

However, with the growing use of such cold-formed steel wall frame systems, it has become important to understand the structural response in fire. In this paper, a full-scale natural fire test on a building constructed entirely of cold-formed steel is described with an 8 m span, height-to-eaves of 2.155 m, length of 10 m with trusses spacing at 2.5 m. The CFS building structure tested had an opening factor of 0.027 $m^{1/2}$ and subjected to a fire load density of 734 MJ/m^2. Two adjacent walls were lined internally with fire resistant lining to achieve a structural fire resistance of 30 minutes (R30) and the fire load was calculated to generate a structural fire severity of 30 minutes; i.e. matching the wall resistance. Thus the two protected walls were expected to remain vertical throughout the fire; the roof was expected to collapse first followed by pulling in of the unprotected walls. The base connections were designed to support an overturning moment generated by 0.5 kPa face loading on the wall during the fire, as is required by UK and New Zealand standard design practice (see Fig. 1). The wall panels are assembled on-site using vertical studs fixed to the bottom and the top tracks by self-drilling / self-tapping screws (Teks). The roof of the building comprised cold-formed steel trusses pinned to the wall

top plates, again connected through Tek screws. The building was designed to achieve a specified performance based on a time equivalent determination of structural fire severity assuming specified levels of roof venting and the actual performance closely matched this.

Design guidance for single storey steel buildings in fire has been focused on the hot-rolled steel. For hot-rolled steel portal frames, the UK Building Regulations [1] make reference to the Steel Construction Institute (SCI) [2] design method (Simms and Newman [3]) for fire boundary conditions; New Zealand has similar guidance. Currently, the SCI design method allows the rafters to be left unprotected, so long as the column bases are designed to resist an overturning moment, calculated in accordance with the SCI design method. The SCI design method makes the assumption that both rafters are heated uniformly. It also assumes that the rafters undergo a symmetrical inward snap-through-buckling collapse mechanism, after which the frame stabilises with the rafters suspended below the columns in catenary action. Wong [4] conducted a fire test on a hot-rolled steel frame with pinned column bases. It was observed by Wong that under the fire, the frame had a tendency to sway sideways. Bong [5] extended the work of Wong [4], developing a beam model of a portal frame building arrangement which included purlins and side rails. An asymmetric sideways sway mode was observed. It is to be mentioned that SCI design guidance presumes a symmetrical collapse mode and does not include asymmetric collapse for hot-rolled steel framed buildings [2]. Song et al. [6] developed a beam model for the frame tested by Wong [4] and were able to predict the behavior of the frame to collapse. Through an FEA study, Rahman et al. [7] showed that the SCI design recommendations may not be adequate and that hot-rolled steel frame may be susceptible to an asymmetric mode of collapse [4].

While numerous researchers have conducted investigations on CFS wall panels in fire, these have been conducted through standard furnace tests, involving an isolated wall panel

placed into a furnace with prescribed support conditions and exposed to the prescriptive Standard Fire temperature-time condition. Neither the 'true' structural behaviour nor the fire conditions are emulated through the furnace tests. Furthermore, in practice, one or more walls are typically close to a boundary and are required to develop a specified fire rating.

In terms of single CFS members subjected to bending under elevated temperatures, significant research is available in the literature, which uses fire furnace tests [8-13]. Whereas, the research on CFS studs and columns were also carried out by Feng [14], Ranawaka [15], Chen and Young [16] and Gunalan [17]. These studies were contributed a better understanding on the behavior of local, distortional and lateral distortional buckling behavior of CFS members. The individual CFS members are traditionally tested by standard fire test using a furnace in laboratory. However, it could be challenging to build a large furnace to test and determine the fire performance of a CFS building.

Law [18] as cited by Bisby et al. [19] addressed the shortcomings of standard fire tests [20] for single elements. As explained by Bisby et al. [19], the standard temperature-time curve is not representative of a natural fire in a real CFS building. Besides the boundary conditions in standard fire tests neglect the structural continuity, restraint, redistribution and membrane actions in actual buildings [19]. It is to be mentioned that the standard fire tests [20] for single members using fire furnace can only demonstrate the local failure of individual members and unable to provide enough information on the collapse of the whole building. The behaviour of individual beam or column members in fire do not include the interaction of members within a structural system, the influence of the semi-rigid connections and the influence of the real supports on the response of the overall system. No tests on CFS trusses have been undertaken. Therefore, tests on individual members give little meaningful information with regard to

overall building behaviour, necessitating fire testing on the whole building to obtain this understanding.

Thus, a full-scale fire test was conducted in this study to investigate the actual performance a CFS building under natural fire. The sequence of progressive collapse was studied in the fire test. Progressive collapse is defined by the initial local failure in a structural member which causes a sequence of failure in other members. Additionally, the side sway collapse of the CFS building may threaten the lives of fire fighters and building occupants during the fire egress, which can't be predicted from a furnace test. Javed et al. [21] and Abreu et al. [22] reviewed the current research on CFS subjected to bending and compression at elevated temperatures. Abreu et al. [22] concluded that there is lack of understanding on the behaviour of CFS building structures in fire. This paper has therefore investigated the collapse behaviour of a CFS building in natural fire through full scale natural fire testing and finite element modelling.

In terms of CFS buildings on fire, Pyl et al. [23] conducted a full-scale test on a portal frame building with insulated composite panels for the walls and roofing and hot-rolled steel gusset plates. The test building was of 8 m span, 20 m length, height-to-eaves of 2.5 m and a frame spacing of 5 m with column bases fixed to pad foundations. A beam idealization of the structure was also presented [23]. However, no allowance in the beam idealization was made for joint strength and stiffness. In terms of developing a numerical model to idealize the behavior of CFS portal frame buildings in fire, a beam model cannot capture the effects of plate buckling that eventually lead to failure. More recently, Johnston et al. [24-26] conducted a full scale fire test on a 10 m span CFS portal frame building, the cold-formed steel portal frame collapsed asymmetrically at 714 ˚C. Johnston et al. [25] also developed a non-linear elasto-

plastic finite-element model, which was validated against the test results of cold-formed steel portal frame building in fire.

Neither, Ply et al. [23] nor Johnson et al. [24-27], however, considered a single-storey cold-formed steel cantilever wall/truss system. In such buildings, unlike portal frames, one or more layers of gypsum board are provided to the walls for protection from fire; the roofs are again typically not protected. Despite the increasing popularity of cold-formed cantilever wall/truss system, there is very limited research on their collapse behavior under elevated temperatures. The issue of understanding the collapse behavior in severe fire of cold-formed steel cantilever wall/truss system, with a mix of protected and unprotected walls and unprotected truss roofs is considered herein.

The results of the full-scale test have been used to validate a non-linear elasto-plastic finite element shell model for cold-formed steel cantilever wall/truss system under elevated temperature. The FEA model comprised a slice through the building containing two trusses and their supporting walls to predict the collapse behaviour of the central part of a portal building remote from the gable walls. Comprehensive finite element modelling of portal frame structures with unprotected steel frames and roof bracing by O'Meagher et al. [28] has shown that modelling a slice of this type of building remote from the gable walls is appropriate to determine the collapse behavioural mechanisms of this type of building. The full geometry of the roof truss was modelled using the finite element software ABAQUS [29]. The collapse temperature predicted by the numerical model is found to be similar to that of the full-scale test; therefore the FE model can be used by engineers to assist in the design of this type of cold-formed steel cantilever wall / truss system in severe fire conditions. The investigation presented herein, can form the basis of a performance based approach for the design of cold-formed steel cantilever wall/truss system in fire boundary conditions.

2 Experimental investigations

2.1 Preamble

The full scale fire test was conducted at Curtin University, Sarawak Campus, Malaysia on 14 October 2015, as a result of the international collaboration between Curtin University Sarawak and The University of Auckland.

2.2 Details of the CFS building

The cold-formed steel cantilever wall/truss system consists of 8 m span, 2.155 m height to eaves and 15-degree roof pitch (see Fig. 1). Such building systems are typical in Malaysia and South East Asia. It was designed to behave in a specified way in a severe fire, with roof venting and partial wall collapse. Fig. 2 shows the CAD drawing of cold-formed steel cantilever wall/truss system investigated herein showing which walls were protected on the inside to achieve a 30 min FRR and which were not protected. The total length of the building length was 10 m; comprising seven frames spaced at 1.667 m. Cold-formed steel channel-sections were used for the entire building with a material grade of G550 steel. The section designation, nominal dimensions and section properties are shown in Table 1. The wall studs and roof trusses were constructed using C07508 lipped channel section, which denotes a section having 75 mm web depth and 0.8 mm thickness. The purlins, side rails and bracing members used C07510 sections.

The eaves and apex joints were formed through a 400 mm × 450 mm cold-formed steel plate with thickness of 3 mm (see Fig. 3(a)) Each joint comprised two rows of 10 × 5.43 mm diameter AS Tek self-drilling fasteners, each 20 mm long. The column bases were constructed using an M12 bolt through a 5 mm thick steel base cleat. Further details on the screw fasteners are given in Table 2.

Figs. 3(b) to 3(e) show the base and wall connection details of the cold-formed steel framing. The cold-formed steel wall bottom track connection comprised two 1.2 mm thick L angle bracket fixed with two rows of AS Tek self-drilling fasteners. The L angle brackets were bolted using a Hilti M12 anchor bolt through the 150 mm thick concrete base. The L angle brackets were used to level and support bottom tracks of the wall and the gap between the track and the concrete base was filled with concrete. Such base connection was design to resist moments resulting from lateral loads applied to the wall in both ambient and elevated temperature.

The cladding comprised 9 mm thick cement board, which was detailed in such a manner to contribute to diaphragm action. This was achieved through the cladding material itself, the boards not being placed overlapped and the screw connections being semi-rigid and limited in number. An opening of 2.5 m wide by 1.9 m high was placed at both gable end frames to simulate a roller shutter door. Along the side of the structure, four openings each of width of 0.6 m and height of 0.875 m high were included. The size of the openings was designed to ensure that there would be sufficient ventilation, without which the fire may have extinguished prematurely.

2.3 Loading, fire source and instrumentation

A load equal to 0.211 kN/m for each truss was applied to the roof. The load comprised self-weights of the cladding, purlins and the weight of the cement bricks. The additional cement brick load was to ensure that collapse of the frame would occur during the fire, to enable subsequent validation of advanced structural models. The load was applied through a 9 mm thick cement board, supported by purlins spanning between adjacent frames. The load ratio for the main structural members was 0.21, where the load ratio is the ratio of the imposed load in

the fire test to the collapse load determined from the ambient temperature test. The collapse load at ambient temperature can be found from Kok and Lau [30].

Timber cribs were stacked to a height of 1.4 m across the entire base of the structure, except for a 1.0 m corridor where the fire was ignited. The total volume of wood was recorded as 5.23 m^3, with a unit weight of 670 kg/m^3. The calorific value of the timber was 16000 kJ/kg. The calorific value of the wood was based on generating a structural fire severity of 30 minutes in accordance with C/VM2 [31], based on roof venting of 20% of the floor area which is standard practice in portal frames with non-fire rated roofs in New Zealand.

Instrumentation to measure steel temperature and displacement were positioned at critical locations around the structure. A centralized timing system was employed where readings for each instrument were taken and recorded at 15 second intervals. Type K thermocouple wires were used, with eight thermocouples connected to the structure. Figs. 4(a) and 4(b) shows the location of thermocouple and laser range target for northern and southern side wall respectively. The notation NT and NL denote the location of thermocouples and laser range targets respectively. Fig. 4(c) illustrates the location of thermocouple for the roof truss. The abbreviation RT denoted as thermocouple location for the central roof truss. Fig. 4(d) shows a typical thermocouple and laser range target position. The cladding was removed locally to expose the steel studs and measurements were taken on the outside flange of the wall studs at height of 2.0 m, 1.6 m and 0.9 m from the base. Two laser range measuring devices were used to measure and record the displacement of the columns and roof truss. The cladding was removed locally to expose the steel structure and measurements were taken on the outside flange of the column at a height of 1.8 m from the base.

2.4 Full scale fire test procedure

2.4.1 Temperature development

The timber was lit at the base of the cribs on one side of the span only, in order to initiate a non-uniform natural fire within the building. Figs. 5(a) and 5(b) shows the ignition and post fire stage, at a time of 2 and 15 minutes from ignition respectively.

Figs. 6(a) and 6(b) show the variation of temperature against time for the thermocouples placed around the wall claddings and roof truss, respectively. The standard ISO time-temperature curve and time-temperature curve are also shown for comparison. Since ISO curve did not consider initial fire growth, the ISO curve has been offset along the x-axis to the point of initial rapid temperature rise. Fig. 6(b) shows the highest peak of temperatures recorded in thermocouple number RT 1, RT 2 and RT 3 are slightly greater than the ISO-834 extended curve. Therefore, the ISO curve used as prediction for any fire scenario is slightly less conservative in this case, as the gradient of the experimental fire curve is less steep than ISO curve. However the fire time temperature characteristics are so different from the ISO curve that it should not be used for this purpose.

The thermocouples recorded the time temperature conditions at ten locations around the structure until the point of collapse. A limitation of the experimental setup was that when the structure collapsed, the screwed connections attaching the thermocouple wire to the steel members failed; readings taken after this point were therefore not valid.

The thermocouples show a slow initial growth up to 400 seconds (or 61 °C), after which the fire growth develops rapidly. It can be noticed the temperatures recorded at point RT1 gave the highest temperature of 765.4 °C at a time of 1060 sec. The temperature then decreased from 765.4°C to 390.8°C at a time of 1350 Sec. The heat loss was due to the spalling of cement roof cladding that allowed extra openings for compartment ventilation, consistent with the 20% roof openings used in the calculation of the structural fire severity. When the combustive material received sufficient air ventilation, the fire was again developed up to second peak temperature

of 567.5 °C at a time of 1320 sec. Finally, the downward slope indicates the decay phase of the fire curve. In this stage, the available fuel for combustion was decreased and hence, temperature dropped.

In addition, Fig. 6(a) shows the heating profile of northern and southern side walls. Thermocouples NT1, NT2 and NT3 are the top, middle and bottom location of northern side wall (without gypsum board). Similarly, thermocouples ST1, ST2 and ST3 represent the top, middle and bottom location of southern side wall (with gypsum board). In the fire test, the gas temperature was observed to be higher at the top of the structure. Therefore, the temperature is decreasing from top to bottom of northern and southern side wall.

The peak temperatures of the northern side wall were much greater than the southern side wall, as expected. The time at each peak temperature for curves NT1, NT2 and NT3 were lagging the curves ST1, ST2 and ST3. Considering the critical thermocouple position NT1 and ST1, the highest temperature recorded in NT1 was 659.1 °C at a time of 1320 sec. whereby, the highest temperature recorded in ST1 was 363.5 °C at a time of 1960 sec. Therefore, the gypsum board protected the cold-formed steel stud from 45% rise in temperature and a time delay of 46%.

2.4.2 Description of collapse

Fig. 7 illustrates the schematic collapse of central part of the structure, demonstrating displacement of the frame with time from ignition. The collapse mode was asymmetric with initial thermal expansion of the frame followed by an inward collapse at 622.5 °C, at a time of 21 min 30 sec from ignition. A fire-induced hinge was formed on the steel studs at a time of 22 min, allowing upper part to rotate around the hinge. This mechanism is referred to the snap-through buckling of steel studs. The location of fire-induced hinge was approximately located

on one third the length of wall stud. The snap-through mechanism was recorded at a time of 35 min.

Fig. 8 shows a photograph of the asymmetric collapse of the cold-formed steel building during the fire**.** Figs. 9(a-d) show failure of the CFS building at different times during the fire test. Fig. 9(d) shows a photograph of the CFS building after fire, in which the buckling of the structural members is evident. Neither the eaves nor the apex screwed joints failed. Instead, failure occurred through buckling in the channel sections, at a distance offset from the joints along the member length. It also shows that the roof is in catenary form which pulls the wall and eventual inward collapse is shown in Fig. 9(d).

Figs. 10(a) and 10(b) show the variation of lateral eaves displacement of the stud at top, middle and bottom level against temperature for the northern and southern side studs of the central frame. Initially, the temperature of the cold-formed steel roof trusses and wall studs increased due to the fire. This heating of the steel caused expansion and resulted in the stud moving laterally outwards (as observed by a negative value on chart). The reduced strength and stiffness of the steel then caused the cold-formed steel channel section to buckle, which led to a sharp asymmetrical inwards movement as the results from progressive collapse of roof trusses.

The curve NT, NL1 shows northern side wall underwent large displacement from 0mm to 399 mm at temperature interval of 410°C to 465°C. The northern wall was stabilized approximately 400 mm at temperature interval of 462°C to 596°C. The highest deformation and temperature recorded in the northern side wall were 453 mm and 622.5°C respectively. The temperature and displacement data beyond the maximum point were not recorded due to the loss of contact between the steel stud and the laser range.

The failure mode of the studs and roof trusses can be seen as asymmetrical, which can be expected since the southern wall was protected by gypsum boards, and fire was non-uniform. For the case of southern side wall, the movement and temperatures of southern wall were lesser than the northern side wall. The protected steel framing in southern side wall connections did not collapse and exhibited the desired behaviour. This shows that the methodology used in determining the structural fire severity and in the design of the fire rated walls and their base connections is sound. Similarly the south side wall did not collapse. This wall was also fire rated and with the semi-rigid base connection fixity.

The highest lateral deformation recorded at the top of the southern side wall (curve ST, SL1) was 230 mm at a temperature of 116°C. Whereby, curve ST, SL1 marked the highest temperature of 363 °C at a displacement of 170 mm. Initially, the southern side wall expanded outwards with a maximum displacement of 10 mm at a temperature of 64°C. At a temperature of 200°C, the southern side wall moved inwards from 10 mm to 82 mm as the northern side wall collapsed from 0 mm to 399 mm at temperature interval of 410°C to 465°C. This is evident that the displacement-time curve shows the collapse at a time of 1080 sec or 18 minutes. Beyond the maximum point, the displacement of the southern side wall moving outwards continuously with increased and decreased temperature of 363°C and 160°C respectively. It is believed that the reduction in southern side wall displacement up to 363°C was due to the collapse of northern side wall. In other words, the inward collapse of northern side wall pushed the southern side wall to move in the outwards direction, then the wall was subsequently pulled slightly inwards by the still attached roof pulling in on the top of the wall. In addition, the steel studs underwent contraction due to cooling from 363°C to 160°C. Finally the peak outwards deflection at the top of the wall may have been generated in part by thermal induced expansion of the wall as a cantilever, following roof collapse, away from the fire. The effects following

roof collapse resulted the southern side wall outwards lateral deflection decreasing during the period between the roof collapse and the end of the fire.

The displacement-time graph of northern side wall was plotted as shown in Fig. 10(a) to illustrate the movement of northern side wall with respect to time. During the ignition phase, the northern side wall did not show any changes up to 600 second or, 10 minutes. The laser range NL3 lost its contact to the wall and only recorded displacement up to 680 seconds. The corner laser range location NL6 and NL7 shows little change up to 1200 seconds until an inward collapse was recorded at 1490 seconds.

At 600 seconds to 920 seconds, the laser range locations NL1, NL2, NL4 and, NL5 show an outward wall movement due to the expansion of cold-formed steel members. The curve NL1 recorded maximum outward movement of 33 mm at 770 seconds or equivalent to 12 minutes and 50 seconds. The northern side wall NL1, NL2, NL4 and, NL5 curves show similar trends of inwards movement beyond 920 seconds. Taking the critical location NL1, the highest point of the wall, shows a gradual inward collapse from 0 mm at 920 seconds, to 400 mm at 1180 seconds. The northern side wall did not collapse directly as the wall stabilized itself within 1180 seconds to 1270 seconds. As the strength of CFS wall studs continuously deteriorated by the fire, the northern side wall was no longer bearing the load transferred from the roof. Eventually, the northern side wall collapsed at 1350 seconds or 22 minutes with an inward deflection of 1300 mm. The structural collapse was triggered by local failures or plastic hinges that formed approximately at one-third of the wall height, which caused an inward-snap through buckling of the wall studs.

Moreover, the southern side wall did not show any changes up to 600 second or, 10 minutes. The laser range targets SL1 to SL5 shown in Fig. 10(b) recorded an outward movement of the wall at 600 seconds to 1030 seconds. SL2 recorded maximum outward

displacement of 14 mm at 840 seconds. The southern side wall SL1 to SL5 curves show similar trends of inwards movement beyond 920 seconds. The southern side wall did not collapse after reached its maximum displacement. Considering the critical location SL1, the highest point of the wall, shows maximum inward displacement of 230 mm at 1430 seconds. After this maximum point, the wall moved outwards gradually at 1430 seconds to 2030 seconds. The movement of the wall remained constant at 160 mm. It is believed the inward collapse of northern side wall had caused the southern side wall moved outwards at 1430 seconds to 2030 seconds.

Figs. 11(a), 11(b) and 11(c) show the final deformed shapes of the northern wall, southern wall and the roof truss, respectively at the end of the fire test. Also shown in Fig. 12, the eve connection failed at the end of the fire test.

3. Numerical investigation

3.1 General

A non-linear elasto-plastic finite element model was developed using ABAQUS [29]. The FEA model comprised a slice through the building containing two trusses and their supporting walls to predict the collapse behaviour of the central part of a portal building remote from the gable walls, based on recommendations from similar scope of modelling undertaken previously [28]. The centre line dimensions of the cross section were used in the FE model. To model a full structure, with possible non-uniform fire temperature distribution is more difficult than modelling an individual member with uniform fire exposure. Therefore, efforts were made to create a simple FEA model on a slice through the building and used uniform fire exposure. Specific modelling techniques are described below.

3.2 Geometry and material properties

Thermal properties of cold-formed steel and gypsum boards are crucial for heat transfer analysis and thermal-mechanical analysis. This includes thermal stress-strain curves, thermal expansion, thermal conductivity, specific heat capacity and density as function of temperature.

For the case of cold-formed steel, the specific heat capacity, thermal expansion and conductivity were adopted from Eurocode 3 Part 1-2 [32] as shown in Fig 13. Various researchers (Zhao et al. [33] S Gunalan [17] S Cheng [10] and RPD Johnston [26]) used the thermal properties of cold-formed steel proposed in the Eurocode 3 Part 1-2 [32] for their FE models. They reported a good correlation between their finite-element and experimental results.

The stress-strain curve obtained from the tensile coupon tests at ambient temperature as shown in Figs. 14(a) and 14(b) were converted to stress-strain curves at elevated temperatures using empirical equations proposed by Kankanamge and Mahendran [34]. This is because similar steel grade and coupon thickness were investigated in this paper. As per the ABAQUS manual [29], the engineering material curve is converted into a true material curve by following the equation below:

$$\sigma_{true} = \sigma(1+\varepsilon) \tag{1}$$

$$\varepsilon_{true(pl)} = \ln(1+\varepsilon) - \frac{\sigma_{true}}{\mathrm{E}} \tag{2}$$

Where E is the Young's Modulus, σ and ε are the engineering stress and strain respectively in ABAQUS [29]. Fig. 14(c) shows the true stress-strain curves at elevated temperatures. The value of Young's modulus used in this study was 200.4 Gpa. Whereas a poison ratio of 0.3 was used in this study [32, 17]. The density of cold-formed steel used was considered as 7850 kg/m^3.

Additionally, the density loss, specific heat capacity and thermal conductivity of the gypsum board was determined from the laboratory tests as shown in Figs. 15(a-c). The values of density loss and specific heat are the outcome of laboratory tests using thermogravimetric analysis and differential scanning calorimetry analysis as shown in Figs. 15(b) and 15(d), respectively. The thermal conductivity curve used for the FE modelling is shown in Fig. 15(e), which was determined using the proposed equation by Rahmanian and Wang [35]. The values of Young's modulus and thermal expansion coefficient were adopted from Cramer et al.[36] as illustrated in Fig. 15(f) and Fig. 15(g), respectively. Poisson ratio of the gypsum board was taken as 0.2 [35]. These values were used in the FE model developed in this study.

3.3 Element type and mesh sensitivity

DS4 shell elements were used for heat transfer analysis as it provides temperature degree of freedom. Appropriate mesh size were determined in order to acquire the accurate results with lower computation time. A finer mesh size provides higher accuracy but requires longer computation time. A convergence study was carried out based on 50 mm, 30 mm, 20 mm and 10 mm mesh size. Across the length and width, a mesh size of 10 mm × 10 mm was used in the FE model, based on the convergence of the model. Number of elements were confirmed through a mesh sensitivity analysis. The FE mesh used in the FE model, is shown in Fig. 16(a).

3.4 Contact modelling

Surface to surface contact was applied to prevent the cold-formed steel member from intersecting to each other during the simulation. It was applied to all of the intersect surfaces in FE model. In order to reduce the computational time, the tangential behaviour of contact surfaces was defined as frictionless. In addition, the normal behaviour of contact surfaces was defined as "Hard Contact".

3.5 Connection modelling

The screw connections in the modelling of CFS cantilever wall / truss system were simplified by using "Fasteners Builder" to provide restraints in the model. The restraints were applied according to the locations of screw in full-scale field test assemblies. The connector type used for screw constraints was a combination of "Cartesian and Rotation". These boundary conditions allow all the relative displacements and rotations of the screw constraint.

3.6 Boundary conditions and load application

Boundary conditions were used in finite element model to identify the values of all basic solution variables such as temperature, displacement, and rotations at nodes. There are two types of boundary conditions used in this model: Thermal boundary condition and mechanical boundary condition. Thermal boundary condition involved the input values of heat conduction, boundary convection, and boundary radiation. Whereby, mechanical boundary condition involved the input of base fixity condition for the CFS cantilever wall / truss system.

Thermal convection and radiation were considered in this study and the coefficient of convection and emissivity were applied onto the FEA model using boundary conditions. Two types of boundary conditions were adopted in this study. For Condition A, cold-formed steel was protected by a layer of gypsum board. The hot surface of gypsum board was considered as exposed surface, while the remaining surfaces were regarded as ambient surfaces. For Condition B, cold-formed steel was directly exposed to fire. Hence all the surfaces of cold-formed steel were considered as exposed surfaces.

Table 3 shows the values of convection coefficient and emissivity used by previous researchers (Semitelos et al. [37], Thomas [38], Rahmanian and Wang [35], Keerthan and Mahendran [39]). It was shown by previous researchers [35, 36-39) that the convection coefficient of 25W/m^2 and 10W/m^2 at exposed and ambient sides are conservative. Therefore,

the coefficient of convection at exposed and ambient surfaces was used as 25W/m^2 and 10W/m^2, respectively in the FE model. As shown in Table 3, the radiation emissivity value considered in the FE model for exposed and ambient surfaces was 0.8. Boundary conditions were used to define the base fixity of the model at the initial state. As shown in Fig. 16 (b), pinned support (U1=U2=U3=0) condition was applied on the bottom trucks of the FE model.

3.7 Analysis procedure

Two types of analyses were carried out for modelling the collapse behaviour of cantilever wall / truss system under fire loading, as discussed below.

3.7.1 Heat transfer analysis

Initially, heat transfer analysis was carried out to simulate the temperature distribution across the members in a transient condition. Heat is transferred via conduction, convection, and radiation. Normally only one side of cold-formed steel wall panel is exposed to fire during a fire event. The temperature on the exposed side of the wall will flow to the ambient side of wall and this phenomenon was known as heat flux. It is the rate of thermal energy flow through a surface per unit of time with the consideration of heat radiation and convection. Heat flux can be calculated using equations 3 and 4.

$$q = R[(T - T_0)^4 - (T_s - T_0)^4] + h(T - T_s) \quad (3)$$

$$R = r\sigma_z \quad (4)$$

Where, R is thermal radiation constant; r is the radiation emissivity; σ_z is known as the Stefan Boltzmann constant (5.68 x 10^{-8} W/m^{2}K^4); T is the surface temperature; T_0 indicates the absolute zero temperature; T_s indicates the sink temperature and h is denoted as the thermal convection coefficient. In the heat transfer analysis, the sink temperature for unexposed surface or ambient surface used was 20 °C. In case of fire exposed surface, the sink temperature followed the temperature-time curve for roof, northern and southern wall recorded in the full-

scale fire test. It is important to note that the temperature against time curve recorded in the full-scale fire test are intended to validate the structural response of the CFS building structure. Fig. 17 shows the temperature against time curves of the roof (RT1), the northern wall (NT1) and, the southern wall (NT2) used in the FE model. ABAQUS software allows the temperature against time curve input via "amplitude" function. The surfaces exposed to fire were assigned in the FE model, based on these amplitude curves (Fig. 17) under the "boundary condition" module in ABAQUS [29].

3.7.2 Thermal-mechanical analysis of cold-formed steel truss

Thermal stress analysis was performed to predict the failure mechanism, time and temperature of the CFS cantilever wall/truss system. Mesh type of S4R was selected for thermal stress analysis. S4R can analyse rotations, local buckling and torsion which is suitable to be used in this study. Two steps were used to perform thermal stress analysis. The first step was loading step to simulate permanent loads while the second step was temperature step. Static general solver was used for the loading step and the time step was input as 1 second. In this step, the weight of bricks, weight of cement claddings and gravitational acceleration were applied. All of the applied loads in step 1 were propagated to step 2. Dynamic implicit incorporated with quasi-static solver was used in step 2 because it can handle the instabilities of structure and able to capture the snap-through effect of cold-formed steel members at elevated temperatures. Quasi-static non-linear analysis with time period of 4800 was used in the dynamic implicit analysis. Maximum number of increments were 1000000 with initial increments of 0.0001 and maximum increment size of 10 was used in the finite element analysis.

3.8 Initial imperfection modeling

Buckling behavior of channel sections are dependent on many factors which include the ratio of length to thickness (L/t), flange width-thickness ratio (B/t) and lip-thickness ratio (C/t). Initial imperfections can be incorporated into the FE model by superimposing local, distortional and global imperfections for accurate FE analysis. For CFS channel columns, Eigenvalue analyses can be performed in ABAQUS [29]. To obtain local and distortional buckling shapes, very small channel thickness should be considered, however, for global buckling shape, large channel thickness can be considered in ABAQUS [29]. For local, distortional and global buckling modes, lowest Eigenmode can be used in ABAQUS [29] to model initial imperfections [40-41]. Silvestre et al. [42] presented a study on the influence of the buckling more shapes (global, local, distortional) on the load carrying capacity of beams beyond the yield load. It was concluded by Silvestre et al. [42] that a larger participation of local and distortional modes in the beam failure mode leads to a higher post-yielding strength reserve, evidencing a higher beam load carrying capacity beyond the yield load. To ensure the reliability of built-up CFS columns, the influence of geometrical imperfections is integrated. On the other hand, Laim and Rodrigues [43] included initial imperfections for the finite element modelling of CFS built-up beams made with open and closed cross-sections. However, RPD Johnston [26] showed that, although initial geometric imperfections effect the ultimate load capacity at ambient temperature, they do not affect the failure temperature of cold-formed steel portal frames in fire. Therefore, initial imperfections were not included in the FE model to avoid the complexity of the analysis.

3.9 Validation of the finite element model

The final collapse mechanism of FE model is shown in Fig. 18. The FE model predicted an asymmetrical collapse at 628.2℃ which was similar to the asymmetrical collapse of full-

scale fire test at 622.5℃ and 22 minutes. On the other hand, the thermal and structural performance of cold-formed steel northern and southern side walls were assessed using temperature-displacement relationships. According to the results of FEA, snap-through buckling was formed at approximately one third from the top of the northern side wall with collapse temperature of 628.2℃ and 22 minutes while the temperature of south wall was 87℃ and able to withstand more than 22 minutes of fire severity. In Figs. 19(a) and 19(b), the failure modes from FEA were compared against the experimental failure modes for both northern and southern walls, respectively. On the other hand, horizontal displacements determined from the FEA, were plotted against the temperature in Fig. 20 for both the northern and southern walls.

The side rails or the top, middle and bottom track played an important role in collapse mechanism of CFS building under fire. In the full-scale fire test, the top rail of northern side wall acted in tension which prevented the wall from out of plane collapse. However, the top rail buckled severely along their length due to being pulled by roof trusses during exposed to high temperature. Fig. 21(a) shows the flange of top rail at the corner was teared due to material degradation at high temperature. Thus, the top rail failed to provide lateral restraint to the wall studs. It was observed from the experiments that the failure of the walls were governed by the buckling of CFS member rather than failure of connections.

In the FE model, when the walls being pulled outwards by roof trusses due to thermal expansion, the top and mid rail temporarily provided lateral restraint to the compression flange. This is evident from the FE results where the thermal stresses are concentrated on the top rail and mid rail at 667 sec as shown in Fig. 21(b). The side rails had the tendency to prevent outward collapse by restraining the vertical CFS studs. However, the top and the mid rail failed to provide lateral restraint to the compression flange when the northern wall collapsed inward. Only the bottom rail provided lateral restrain to the north wall as it did not buckle severely.

This is because most of the heat was accumulated in the roof and knee level and hence, the bottom rail was less vulnerable to fire. For the southern wall, all the side rails provided lateral restraint to the vertical studs as it was protected by the gypsum board.

The FE model developed in this study, was able to simulate the performance of cold-formed steel cantilever wall/truss system at elevated temperatures. The FEA results were in good correlation with the full-scale fire test results, in terms of failure modes, rotational displacement and collapse temperature. Besides, gypsum board has significantly improved the thermal and structural performance of cold-formed steel wall panel assemblies.

4. Conclusions

This paper has described the results of a full-scale natural fire test on a single storey cold-formed steel building, designed to behave in a specified way in a severe fire, both with and without gypsum board. A non-linear elasto-plastic FEA model was also developed, which comprised a slice through the building containing two trusses and their supporting walls to predict the collapse behaviour of the central part of a portal building remote from the gable walls. The collapse temperature of the building from the fire test and that predicted using the finite element shell model are 622.5 °C and 628.2 °C, respectively. From the results of the investigations carried out, the following conclusions are made:

(1) The CFS building behaved as predicted throughout the fire, with roof collapse occurring some 8 minutes after significant fire growth commenced, followed by pull-in failure of the non-fire rated walls.

(2) Failure of the CFS cantilever wall/truss system is not due to failure of the screws.

(3) The CFS cantilever wall/truss system collapsed inward asymmetrically at 622.5 °C and, at a time of 21 min 30 sec.

(4) The fire rated south wall, was stable and remained vertical during the fire to resist the 0.5 kPa load as the linings protected the wall, studs and base connections from high temperature. These fire rated walls would have prevented the outward collapse hence spread of the fire to the adjacent buildings. The same resistance didn't occur on the unlined north and east walls and the roof which was also unlined and which collapsed during the fire as expected.

(5) This failure was governed by an inward snap-through of wall studs at one-third of the wall height.

(6) The walls protected by gypsum did not collapse in the end of the test. A layer of 15mm gypsum board protected the cold-formed steel stud in the South wall from 45% rise in temperature and a time delay of 46%.

(7) The semi-rigid connections at the base of these walls, which were designed to resist an overturning moment from 0.5 kPa applied to the wall panel in either direction, were satisfactory in maintaining the walls upright after the roof collapsed.

(8) The finite element model closely matched the experimental behaviour. Therefore the FE model can be useful in understanding and predicting the behaviour of this type of building in severe fire conditions.

Further research will investigate the effect of initial imperfections and quantify actual base fixity. The first author is currently investigating the effect of different material properties of CFS and gypsum board, thickness of primary structural members and effect of joint stiffness though an extensive parametric study using the FE model described in this paper. The aim of the parametric study is to develop a performance based design method for CFS cantilever wall/truss system in fire boundary conditions, which can be used by researchers and practicing engineers.

Acknowledgements

The authors would like to acknowledge gratefully the financial support from the ICE Research and Development Fund, IStructE Research Fund, and EcoSteel Sdn Bhd.

References:

[1] HMG (Her Majesty's Government) (2006) Approved Document B: Fire Safety – Volume 2, Buildings Other Than Dwelling houses. The Building Regulations 2010 (for use in England). NBS, London, UK.

[2] SCI P165, Building Design using Cold Formed Steel Sections: Construction Detailing and Practice, P.J. Grubb and R.M. Lawson, Editors. 1997, The Steel Construction Institute: Ascot, UK.

[3] Simms W and Newman G (2002) Single-Story Steel Framed Buildings in Fire Boundary Conditions. The Steel Construction Institute, Berkshire, UK, SCI Publication P313.

[4] Wong SY (2001) The Structural Response of Industrial Portal Frame Structures in Fire. PhD thesis, University of Sheffield, Sheffield, UK.

[5] Bong MW (2005) Structural Fire Performance of Steel Portal Frame Buildings. MSc thesis, University of Canterbury, Canterbury, New Zealand.

[6] Song Y, Huang Z, Burgess I and Plank R (2009) The behaviour of single-storey industrial steel frames in fire. International Journal of Advanced Steel Construction 5(3): 289–302.

[7] Rahman M, Lim JBP, Xu Y et al. (2013) Effect of column base strength on steel portal frames in fire. Proceedings of the Institution of Civil Engineers – Structures and Buildings 166(4): 197–216, http://dx.doi.org/10.1680/stbu. 11.00040.

[8] Kankanamge ND and Mahendran M (2008) Numerical studies of cold-formed steel beams subject to lateral-torsional buckling at elevated temperatures. In Fifth International Conference on Thin-walled Structures, Brisbane, Australia (pp. 737-744).

[9] Laím L, Rodrigues JP, and da Silva LS (2013) Numerical analysis of cold-formed steel beams in fire. In Proceedings of the 13th International Conference and Exhibition on Fire and Materials, San Francisco, USA (pp. 163-174).

[10] Cheng S (2015) Fire performance of cold-formed steel sections. (Ph.D.), Plymouth University.

[11] Martins AD, Camotim D, Dinis PB, and Young B (2015, November) Local–Distortional Interaction in Cold-formed Steel Columns: Mechanics, Testing, Numerical Simulation and Design. In Structures (Vol. 4, pp. 38-57). Elsevier

[12] Landesmann A and Camotim D (2016) Distortional failure and DSM design of cold-formed steel lipped channel beams under elevated temperatures. Thin-Walled Structures, 98, 75-93.

[13] Feng M, Wang YC, and Davies J M (2003) Structural behaviour of cold-formed thin-walled short steel channel columns at elevated temperatures. Part 2: Design calculations and numerical analysis. Thin-Walled Structures, 41(6), 571-594.

[14] Feng M (2004) Numerical and experimental studies of cold-formed thin-walled steel studs in fire. PhD Thesis, The University of Manchester.

[15] Ranawaka T (2006) Distortional buckling behaviour of cold-formed steel compression members at elevated temperatures. PhD Thesis, Queensland University of Technology.

[16] Chen J and Young B (2007) Experimental investigation of cold-formed steel material at elevated temperatures. Thin-Walled Structures, 45(1), 96-110.

[17] Gunalan S (2011) Structural behaviour and design of cold-formed steel wall systems under fire conditions. PhD Thesis, Queensland University of Technology.

[18] Law M (1981) Designing fire safety for steel – recent work. Proceedings of the ASCE Spring Convention. American Society of Civil Engineers, New York, 11–15 May 1981.

[19] Bisby L, Gales J, and Maluk C (2013) A contemporary review of large-scale non-standard structural fire testing. Fire Science Reviews, 2(1), 1.

[20] ISO (1999) ISO 834: Fire Resistance Tests - Elements of Building Construction. Geneva: International Standards Office.

[21] Javed MF, Hafizah N, Memon SA, Jameel M, and Aslam M (2017) Recent research on cold-formed steel beams and columns subjected to elevated temperature: A review. Construction and Building Materials, 144, 686-701.

[22] Abreu JCB, Vieira LM, Abu HMH, and Schafer BW (2014) Development of performance-based fire design for cold-formed steel. Fire Science Reviews, 3(1), 1-15.

[23] Pyl L, Schueremans L, Dierckx W and Georgieva I (2012) Fire safety analysis of a 3-D frame structure consisting of cold-formed sections; numerical modelling versus experimental behaviour based on a full-scale fire test. Thin-Walled Structures 61: 204–212.

[24] Johnston RPD, Sonebi M, Lim JBP, Armstrong CG, Wrzesien AM , Abdelal G , Hu Y (2015) The collapse behaviour of cold-formed steel portal frames at elevated temperatures, Journal of Structural Fire Engineering 6 (2): 77–102.

[25] Johnston RPD, Lim JBP, Lau HH, Xu Y, Sonebi M, Armstrong CG, Switzer C, Mei CC (2014) Cold-formed steel portal frames in fire: Full-scale testing and finite element analysis, The Structural Engineer 92(10): 44-50.

[26] Johnston RPD (2015) Investigation of cold-formed steel portal frames at ambient and elevated temperatures. PhD thesis, Queen's University Belfast, Belfast, UK.

[27] Johnston RPD, Lim JBP, Lau HH, Xu Y, Sonebi M, Armstrong CG, Mei CC (2016) Finite-element investigation of cold-formed steel portal frames in fire, Proceedings of the Institution of Civil Engineers – Structures and Buildings 169(1): 3–19.

[28] O' Meagher, AJ et.al. (1990) Fire Protection of Steel Framing – AUBRCC Research Report AP25. BHP Research and New Technology. Melbourne, Australia.

[29] ABAQUS Analysis User's Manual-Version 6.14-2. ABAQUS Inc., USA, (2018).

[30] Kok KY and Lau HH (2018) Experimental investigation into cold-formed steel roof trusses. In Proceedings of the International Conference on Engineering Research and Practice for Steel Construction (ICSC), Hong Kong, 5th to 7th September, 2018.

[31] C/VM2 Framework for fire safety design (2013) Ministry for Building, Innovation and Employment, Wellington, New Zealand.

[32] European Committee for Standardization (CEN) (2005) Design of steel structures—Part 1-2: General rules—Structural fire design. Eurocode 3.

[33] Zhao B, Kruppa J, Renaud C, O'Connor M, Mecozzi E, Apiazu W, and Kaitila O (2005) Calculation rules of lightweight steel sections in fire situations. EUR (21426), 1-226.

[34] Kankanamge ND and Mahendran M (2011) Mechanical properties of cold-formed steels at elevated temperatures. Thin-Walled Structures 49(1): 26–44.

[35] Rahmanian I and Wang YC (2012) A combined experimental and numerical method for extracting temperature-dependent thermal conductivity of gypsum boards. Construction and Building Materials, 26(1), 707-722.

[36] Cramer SM, Friday OM, White RH, and Sriprutkiat G (2003) Mechanical properties of gypsum board at elevated temperatures. In Fire and materials 2003: 8th International Conference, January 2003, San Francisco, CA, USA. London: Inter science Communications Limited, c2003: pages 33-42.

[37] Semitelos GK, Mandilaras ID, Kontogeorgos DA and Founti MA (2014) Simplified correlations of gypsum board thermal properties for simulation tools. Fire and Materials.

[38] Thomas, G. (2002). Thermal properties of gypsum plasterboard at high temperatures. Fire and Materials, 26(1), 37-45.

[39] Keerthan P and Mahendran M (2012) Numerical modelling of non-load-bearing light gauge cold-formed steel frame walls under fire conditions. Journal of Fire Sciences, 30(5): 375-403.

[40] Kherbouche S and Megnounif A (2019) Numerical study and design of thin walled cold formed steel built-up open and closed section columns. Engineering Structures 179 (15): 670–682.

[41] Roy K, Mohammadjani C and Lim JBP (2019) Experimental and numerical investigation into the behaviour of face-to-face built-up cold-formed steel channel sections under compression. Thin-Walled Structures 134: 291-309.

[42] Silvestre N, Abambres M, Camotim D (2018) Influence of the deformation mode nature on the 1st order post-yielding strength of thin-walled beams. Thin-Walled Structures 128: 71-79.

[43] Laim L and Rodrigues JPC (2018) Fire design methodologies for cold-formed steel beams made with open and closed cross-sections. Engineering Structures 171: 759-778.

List of tables

Table 1: Measured specimen dimensions of the channel sections used in the CFS building
Table 1: Fastener details
Table 3: Convection coefficients and radiation emissivity used in the FE model from previous researchers

Table 1 Measured specimen dimensions of the channel sections used in the CFS building

Section Designation	Web depth (mm)	Flange (mm)	Thickness (mm)	Lip length (mm)
C07510	75	40	1.0	14
C07508	75	40	0.8	14

Table2 Fastener details

Diameter	Gauge #12 (5.43mm diameter)
Thread form	14 Threads per inch
Drive	Hex Head 5/16 inch
Length	20 mm
Drill point	6.0 mm length / 4.50mm dia.
Type of steel	C 1022 Steel, Hardened heat treated
Single shear	9.0 kN
Torsion	13 Nm

Table 3 Convection coefficients and radiation emissivity used in the FE model from previous researchers

Previous researchers	Convection coefficient at the ambient side (W/m^2)	Convection coefficient at the exposed side (W/m^2)	Radiation emissivity at ambient side -	Radiation emissivity at exposed side -
Semitelos et al. [37]	Eliminated this parameter by directly input exposed surface temperature	10	0.9	Eliminated this parameter by direct input exposed surface temperature
Rahmanian and Wang [35]	4	25	0.8	0.8
G Thomas [38]	9	25	0.6	0.8
Keerthan and Mahendran [39]	10	25	0.9	0.9

List of figures

Fig. 1: Photograph of the cold-formed steel building investigated in this paper

Fig. 2: CAD drawing of cold-formed steel building investigated in this paper;

(a) Pan view
(b) Front view (elevation)

Fig. 3: Connection details

Fig. 4: Instrumentation used in the full scale fire test;

(a) Northern side wall (Which did not have gypsum board lining) thermocouple NT1 to NT3 and laser range target NL1 to NL7

(b) Southern side wall (Which did not have gypsum board lining to give a 30 minute FRR) thermocouple ST1 to ST 3 and laser range target SL1 to SL7
(c) Thermocouple RT1 to RT3 on central roof truss
(d) A typical thermocouple and laser range target position

Fig. 5: Fire development at different stages of the fire test;

(a) Ignition stage at 2 min
(b) Fire development at 15 min 20 sec

Fig. 6: Temperature versus time curves of northern, southern side wall and roof truss;

(a) Temperature versus time curves of northern and southern side wall
(b) Temperature versus time curves of roof truss

Fig. 7: Deformations of cold-formed steel cantilever wall/truss system

Fig. 8: Assymetrical collapse of the cold-formed steel building under fire

Fig. 9: Failure of the CFS building at different time during the fire test;

(a) Truss collapsed at 25 min 20 sec
(b) Deformed shape of structure at 26 min
(c) Deformed shape of structure at 38 min
(d) Final deformed shape of the cold-formed steel building at the end of fire test

Fig. 10: Displacement verses time profile for northern and southern side walls;

(a) Displacement verses time profile for northern side wall
(b) Displacement verses temperature profile for southern side wall

Fig. 11: Final deformed shapes of northern and southern side wall;

(a) Final deformed shape of north wall
(b) Final deformed shape of south wall
(c) Final deformed shape of the roof truss

Fig. 12: Eave connection failed

Fig. 13: Thermal properties of the cold-formed steel used in the FE model

Fig. 14: Stress-strain curves at ambient and elevated temperatures

Fig. 15: Thermal properties of the gypsum board used in the FE model

Fig. 16: Details of the FE model for cold-formed steel cantilever wall/truss system;

(a) FE meshing
(b) Boundary conditions applied in the FE model

Fig. 17: Temperature against time curves used in FE model

Fig. 18: Final collapse mechanism of FE model

Fig. 19: Comparison of FEA and experimental failure modes;

(a) Northern wall
(b) Southern wall

Fig. 20: Horizontal displacement against temperature graph

Fig. 21: Tearing failure and thermal stress concentration on the northern wall at 667 sec

Fig. 1: Photograph of the cold-formed steel building investigated in this paper

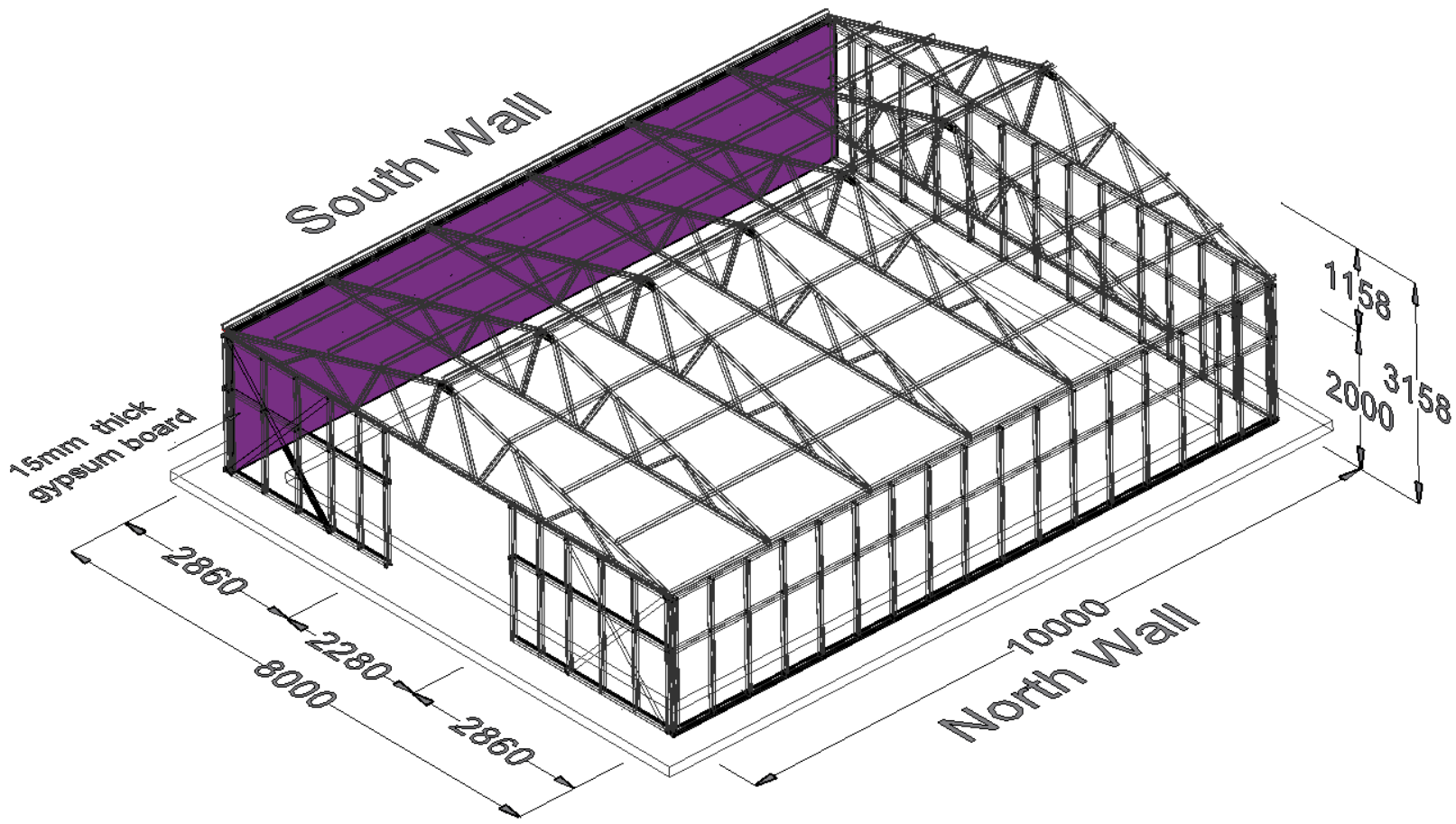

(a) Plan view

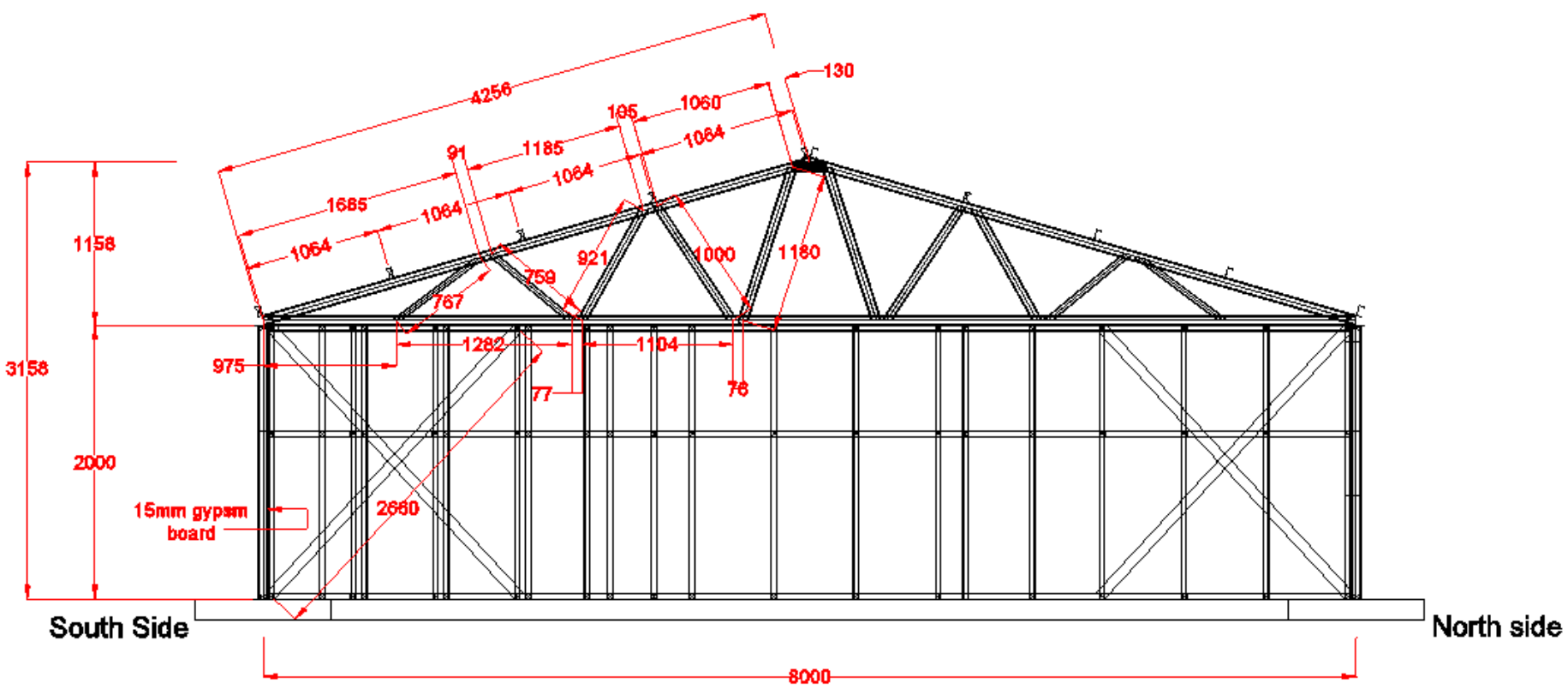

(b) Front view (elevation)

All dimensions in mm

Fig. 2: CAD drawing of cold-formed steel building investigated in this paper

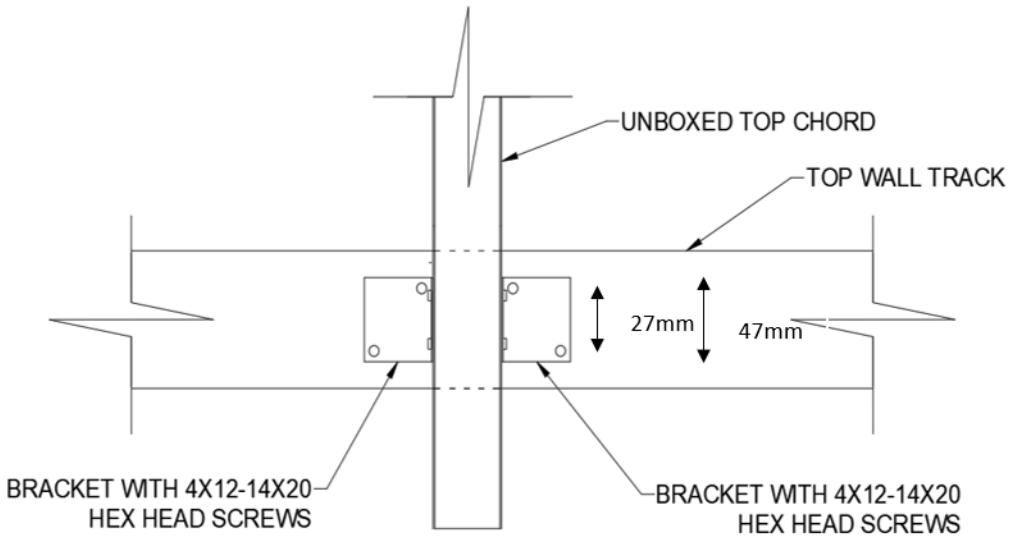

(i) Plan view of roof truss to top track connection

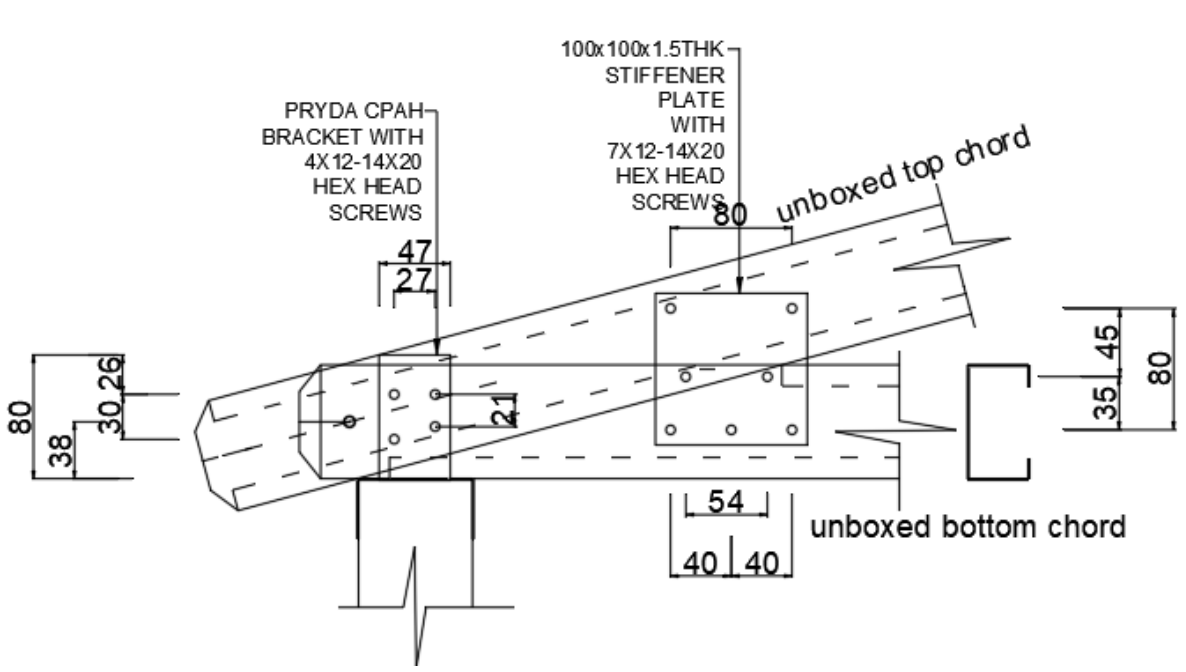

(ii) Side view of eave connection

(iii) Connection between roof and top track

(iv) Eave connection

(v) Apex connection

All dimensions in mm

(a) Roof connection details

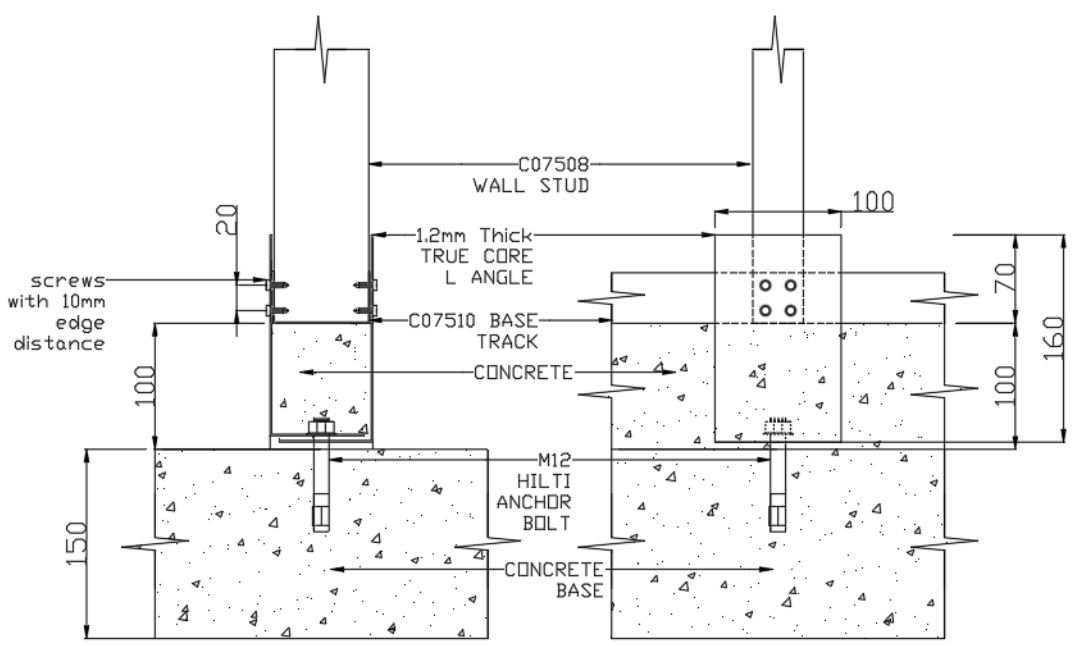

(i) Front view (ii) Side view

(b) Base connection details

(c) Base connection of wall framings

(d) Base connection on site

(e) Base connection after filled with concrete

Fig. 3: Connection details

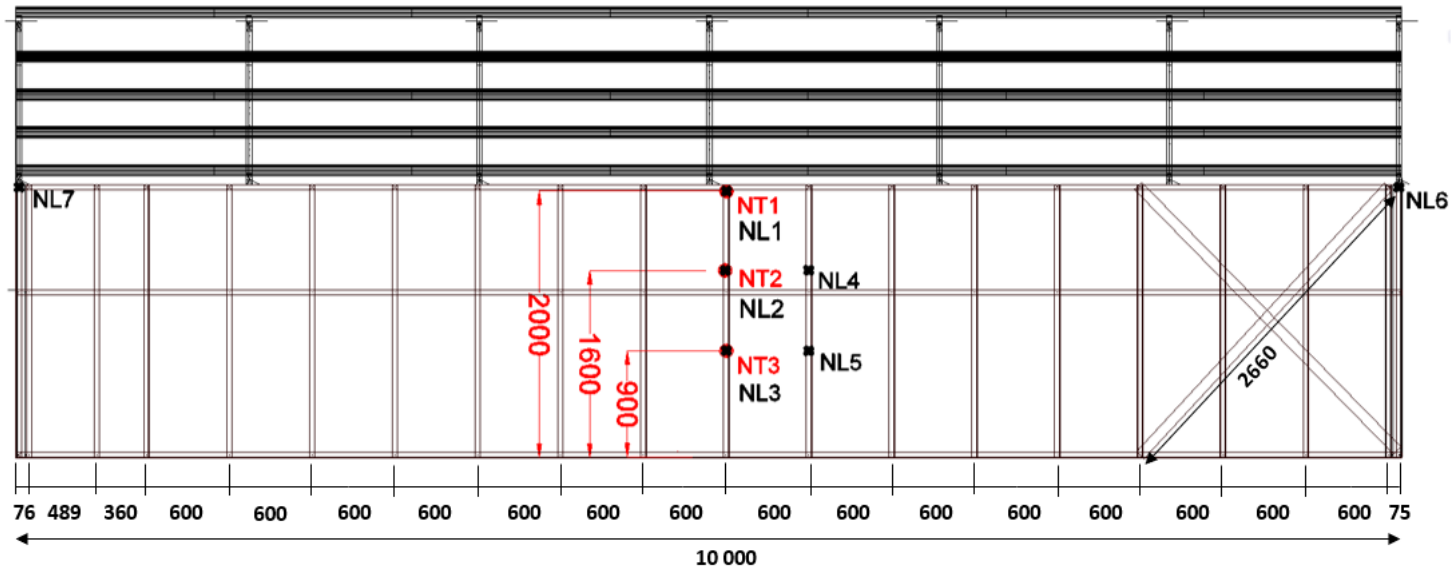

(a) Northern side wall (Which did not have gypsum board lining) thermocouple NT1 to NT3 and laser range target NL1 to NL7

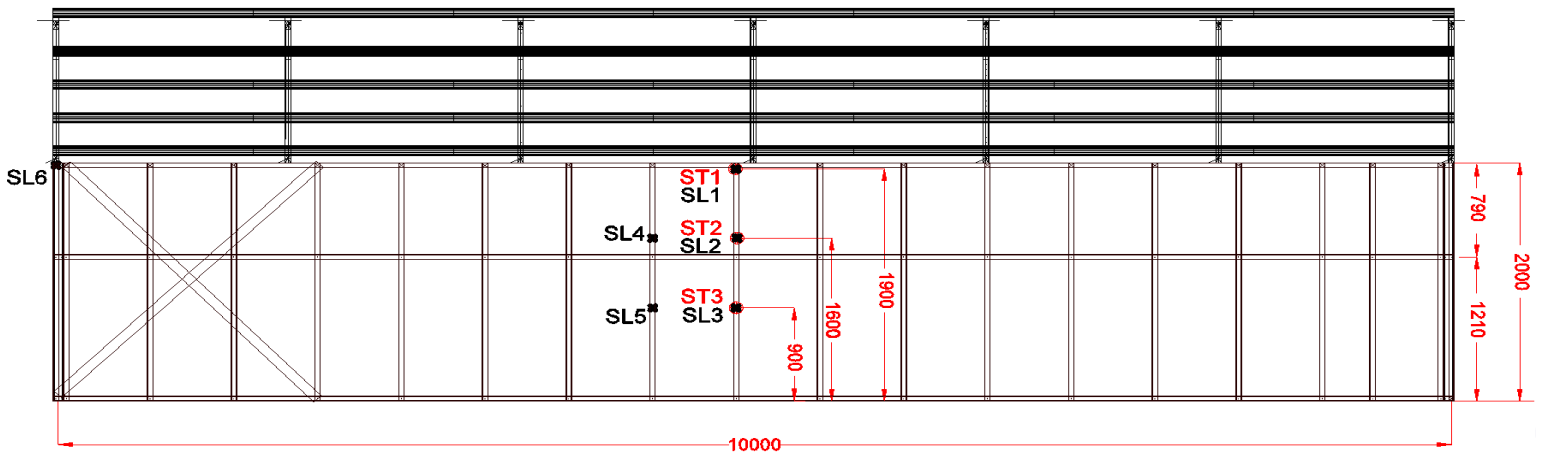

(b) Southern side wall (With gypsum board lining to give a 30 minute FRR) thermocouple ST1 to ST 3 and laser range target SL1 to SL7

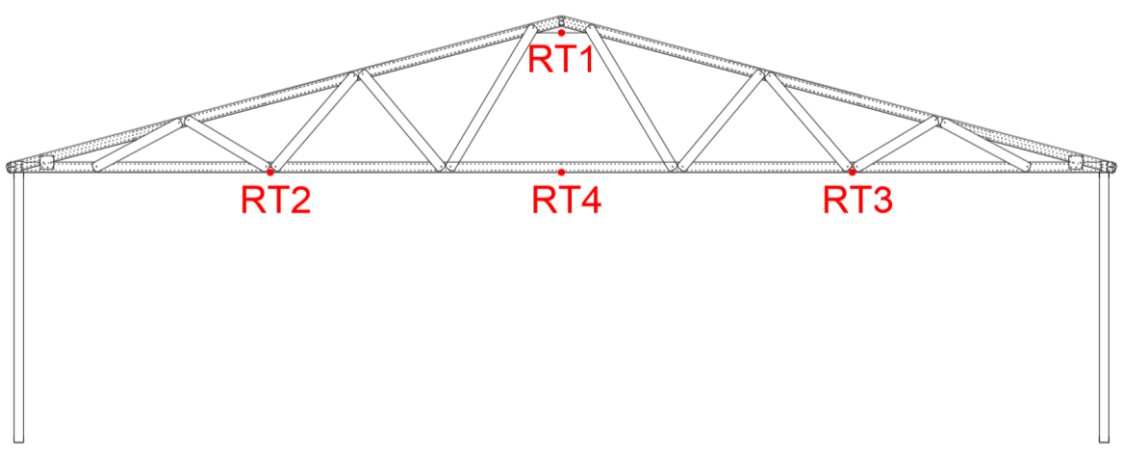

(c) Thermocouple RT1 to RT3 on central roof truss

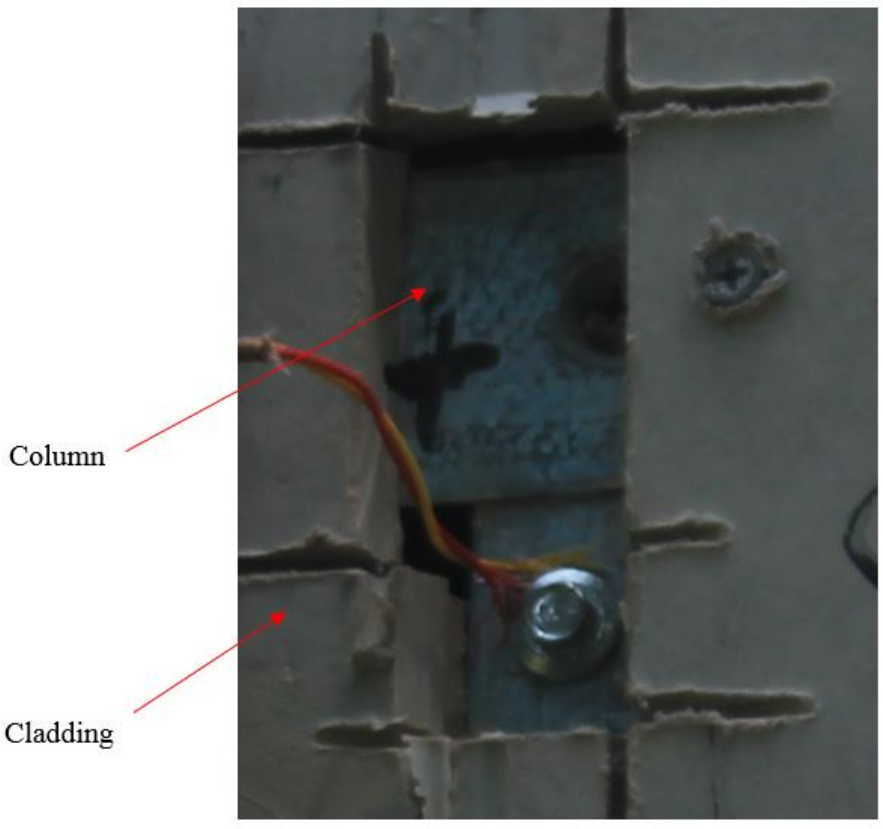

(d) A typical thermocouple and laser range target position

Fig. 4: Instrumentation used in the full scale fire test

(a) Ignition stage at 2 min

(b) Fire development at 15 min 20 sec

Fig. 5: Fire development at different stages of the fire test

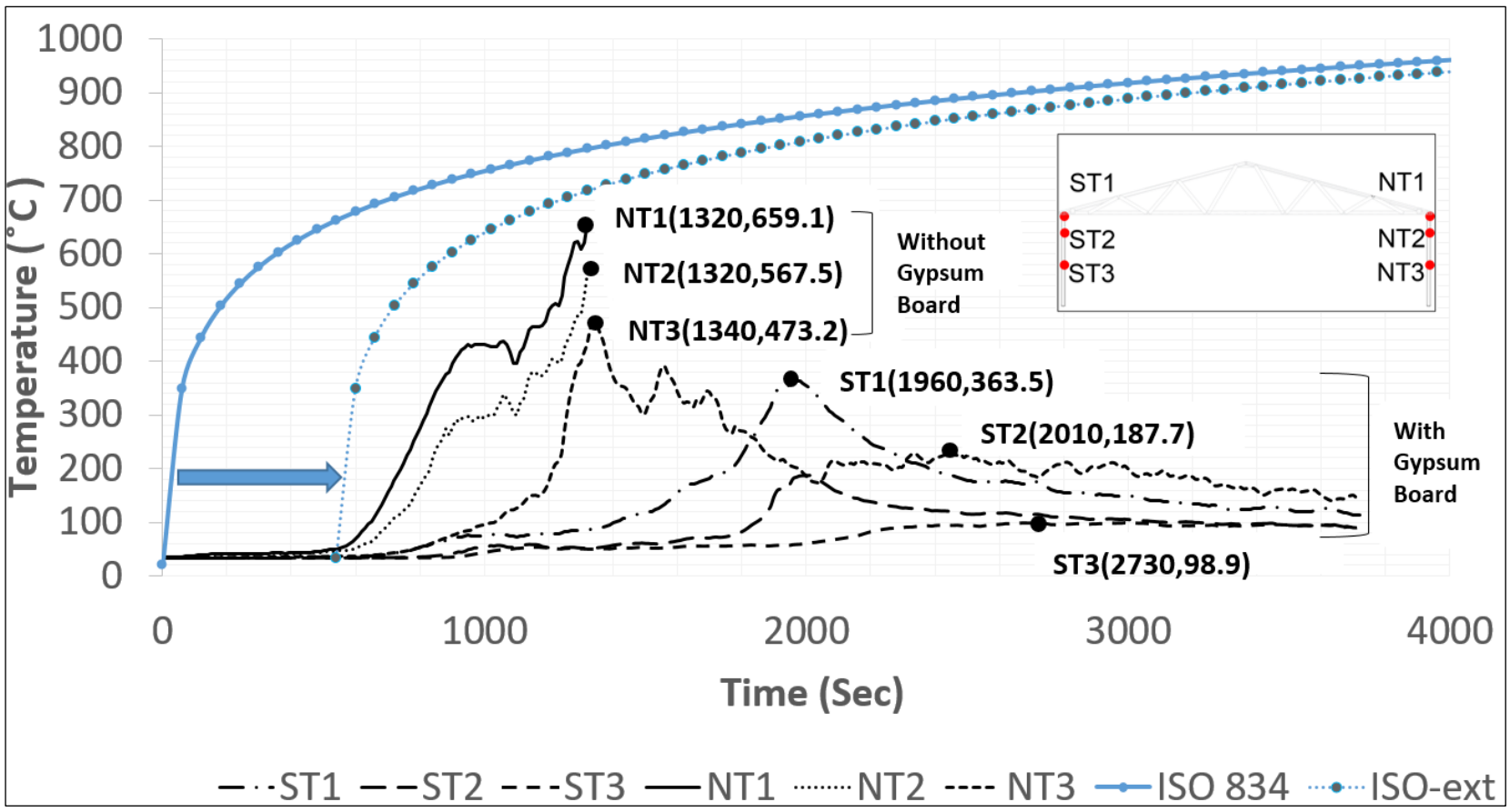

(a) Temperature versus time curves of northern and southern side wall

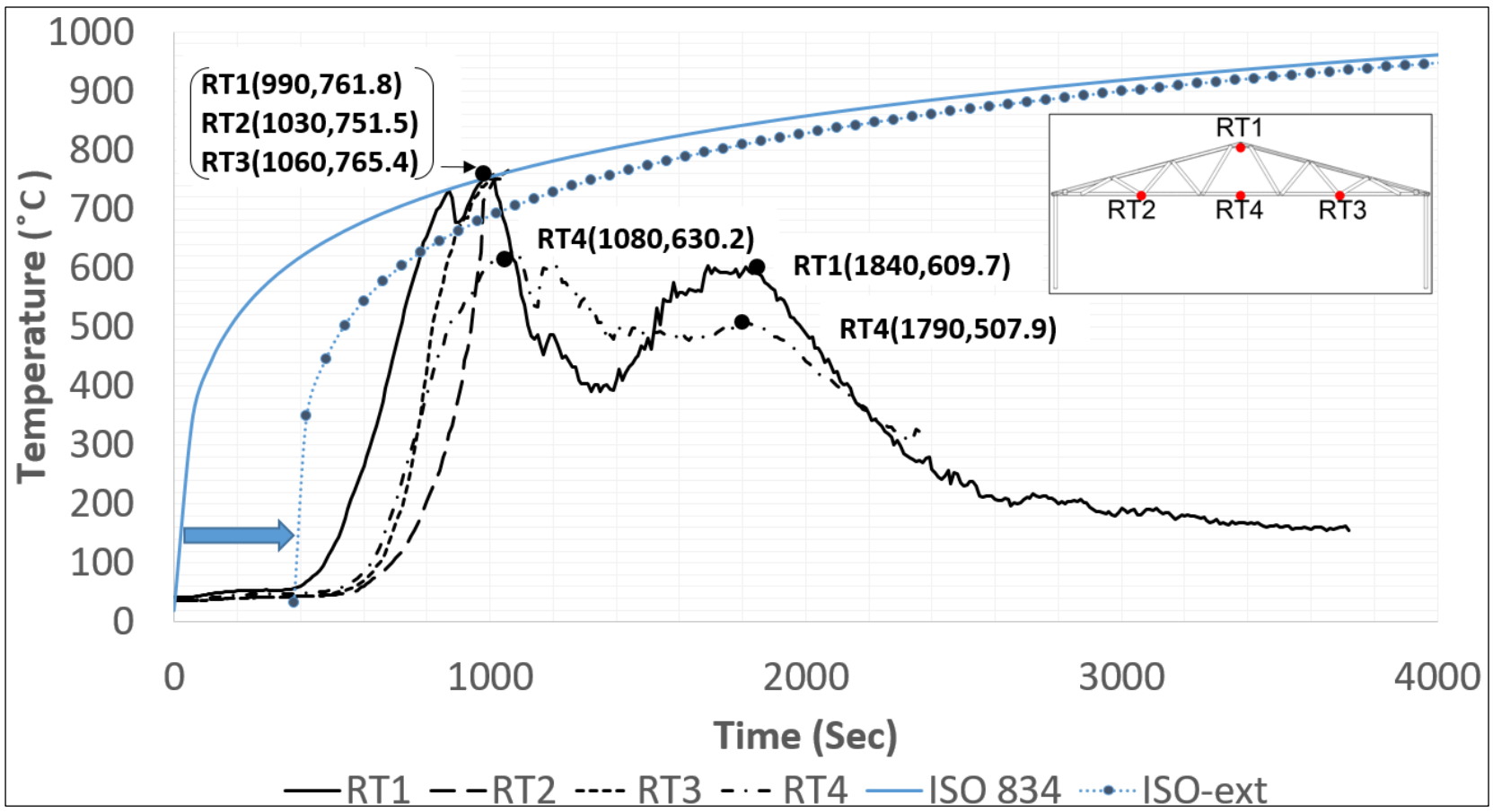

(b) Temperature versus time curves of roof truss

Fig. 6: Temperature versus time curves of northern, southern side wall and roof truss

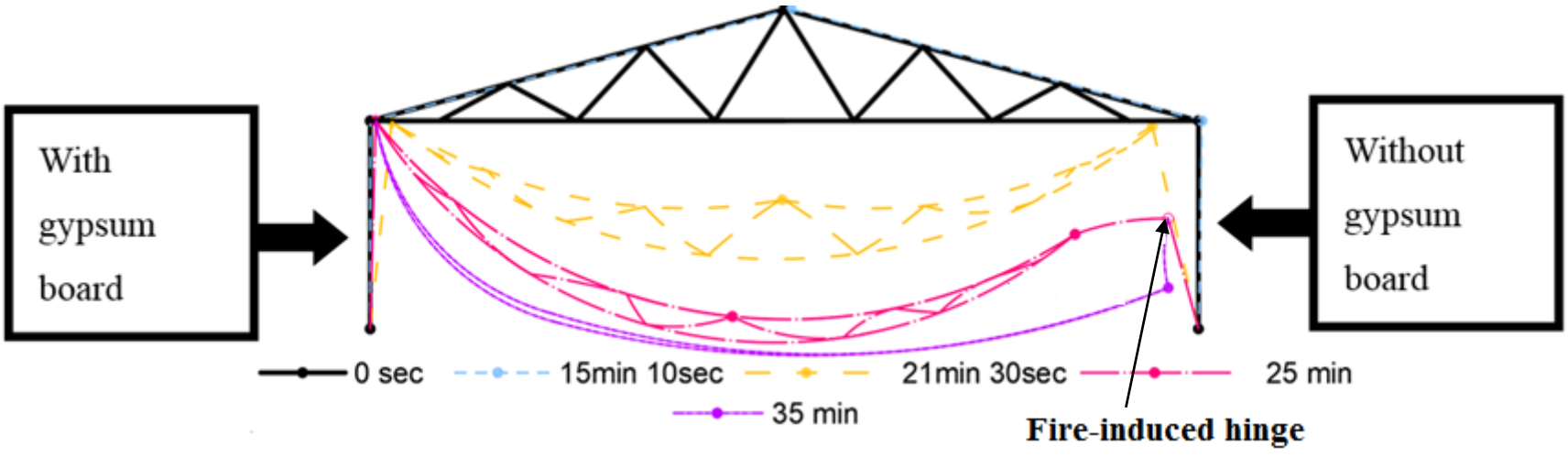

Fig. 7: Deformations of cold-formed steel cantilever wall/truss system

Fig. 8: Assymetrical collapse of the cold-formed steel building under fire

(a) Truss collapsed at 25 min 20 sec

(b) Deformed shape of structure at 26 min

(c) Deformed shape of structure at 38 min

(d) Final deformed shape of the cold-formed steel building at the end of fire test

Fig. 9: Failure of the CFS building at different time during the fire test

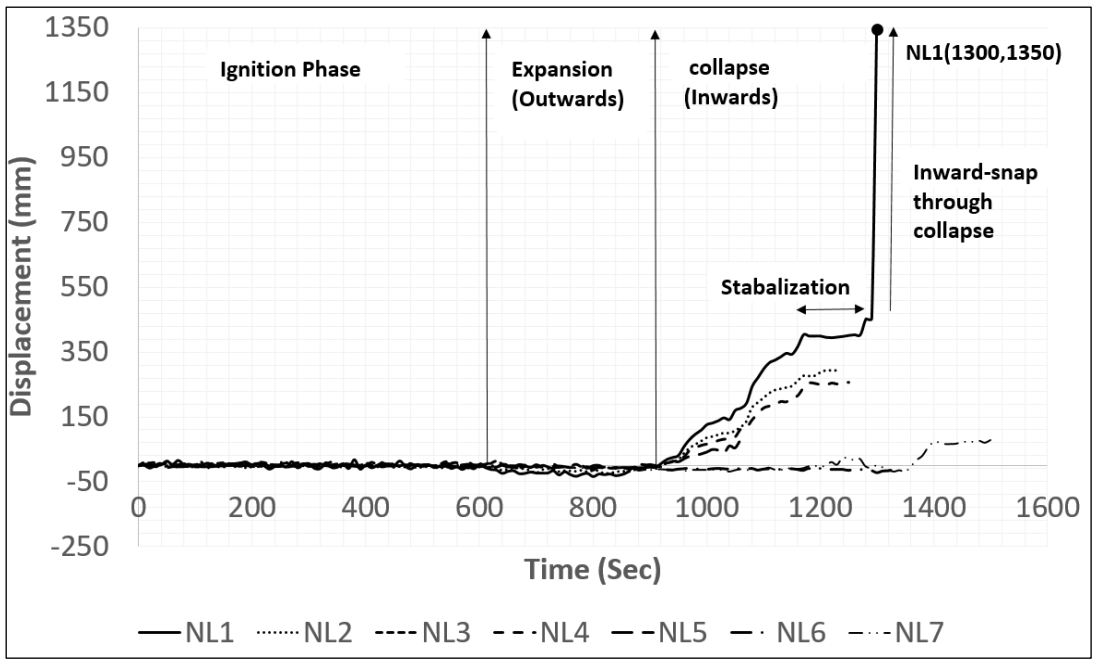

(b) Displacement verses time profile for northern side wall

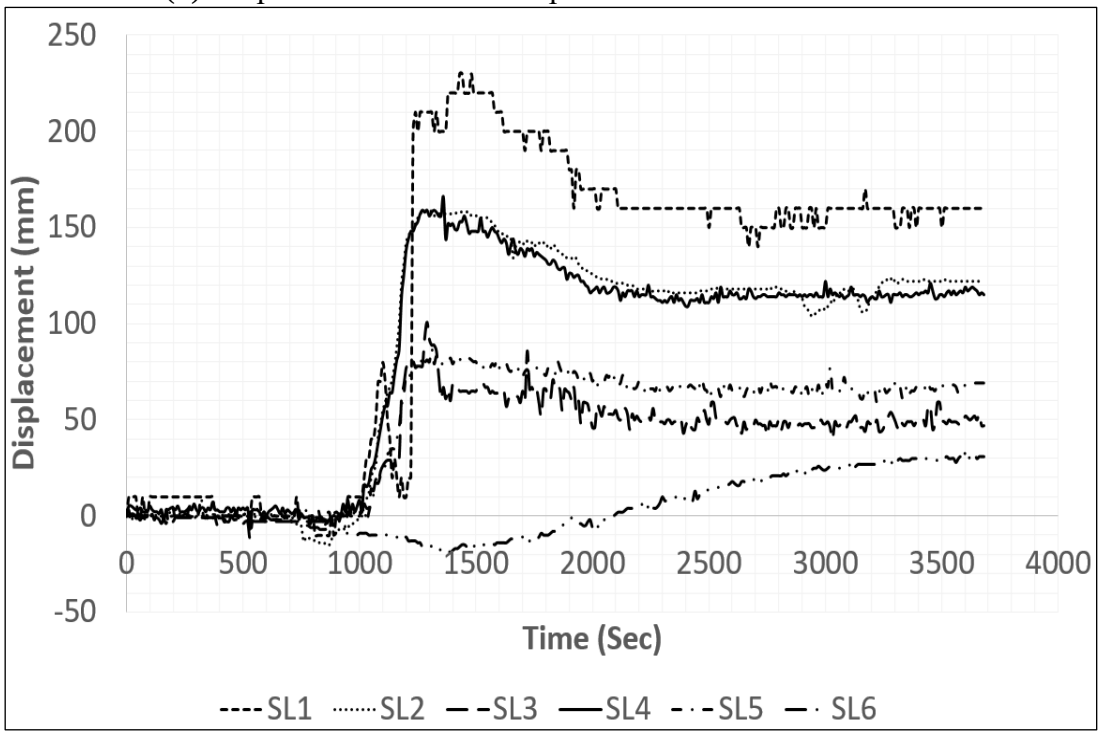

(b) Displacement verses temperature profile for southern side wall

Fig. 10: Displacement verses time profile for northern and southern side walls

(a) Final deformed shape of north wall

(b) Final deformed shape of south wall

(c) Final deformed shape of the roof truss

Fig. 11: Final deformed shapes of northern and southern side wall

Fig. 12: Eave connection failed

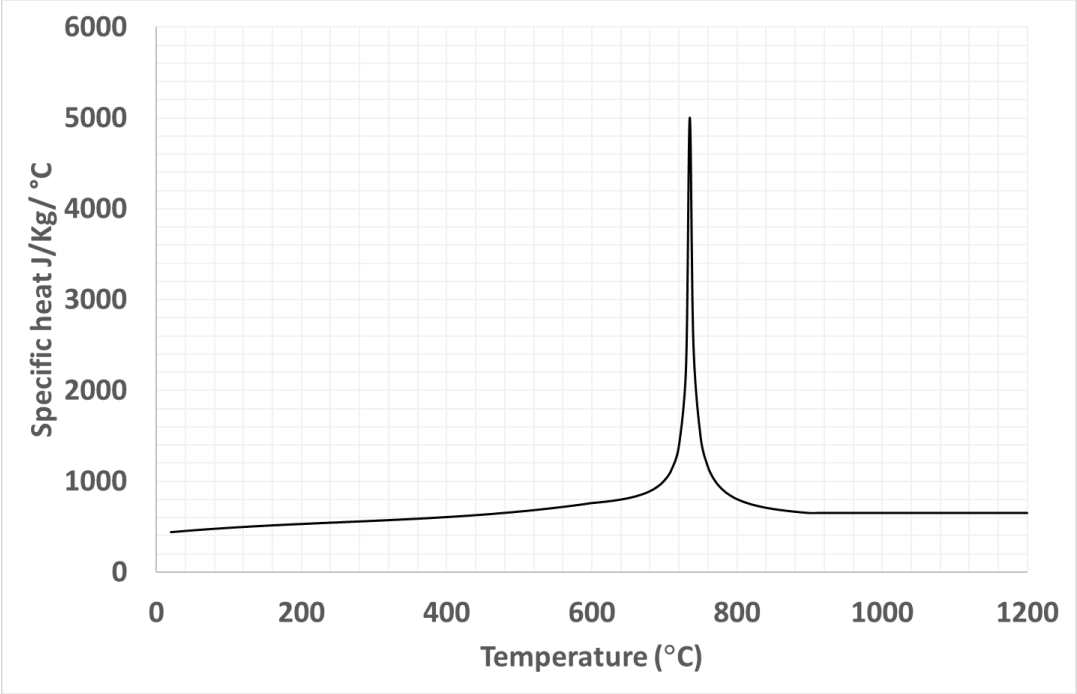

(a) Specific heat of cold-formed steel at elevated temperatures (CEN, 2005)

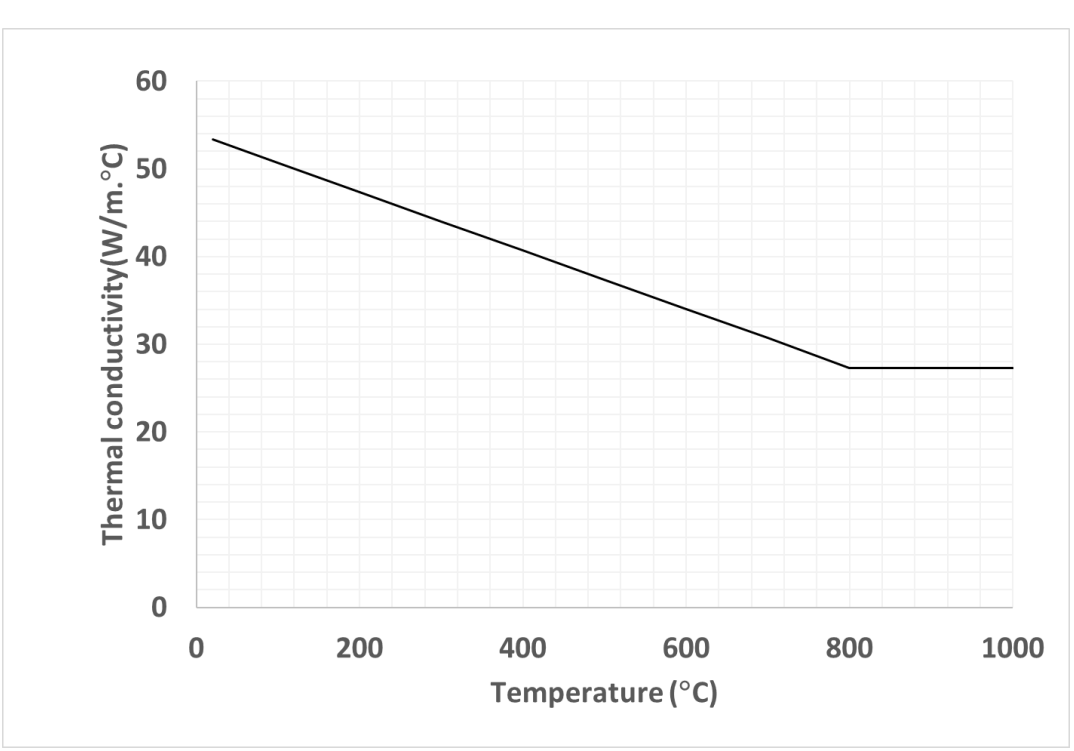

(b)Thermal conductivity of cold-formed steel at elevated temperatures (CEN, 2005)

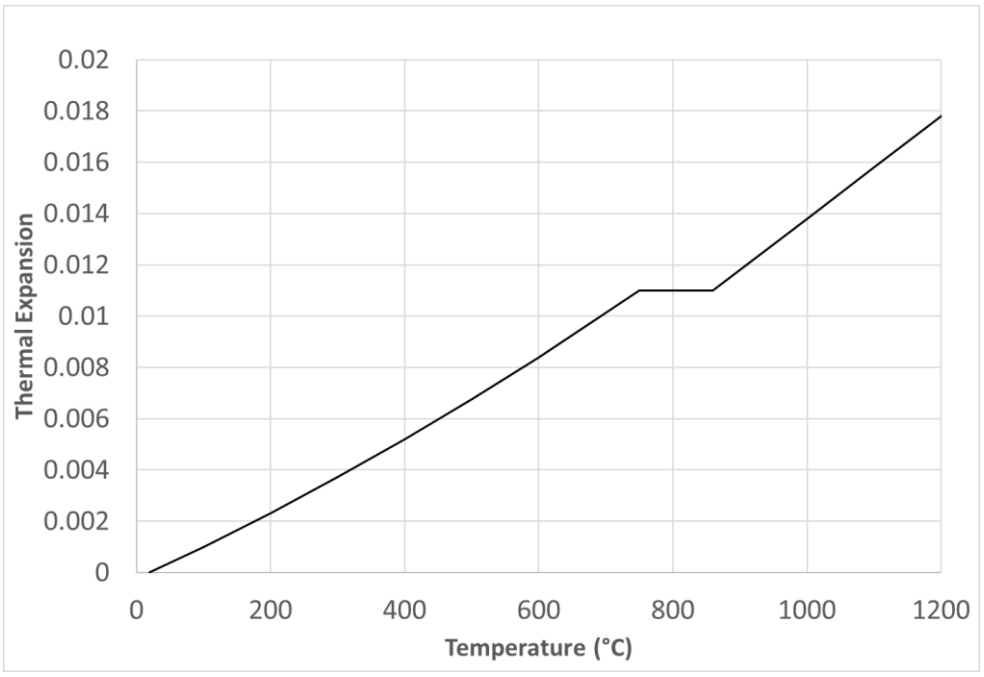

(c) Thermal expansion of cold-formed steel at elevated temperatures (CEN, 2005)

Fig. 13: Thermal properties of the cold-formed steel used in the FE model

(a) Tensile coupon test at ambient temperature

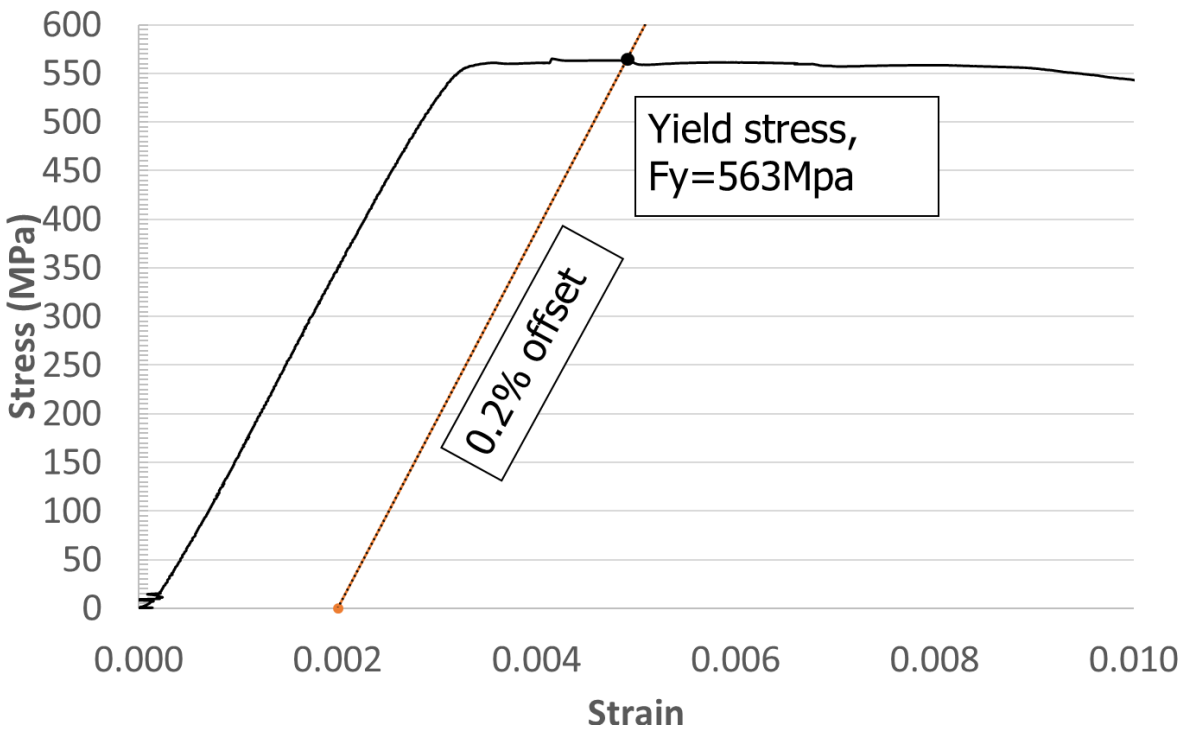

(b) Stress-strain curve of G550 cold-formed steel at ambient temperature

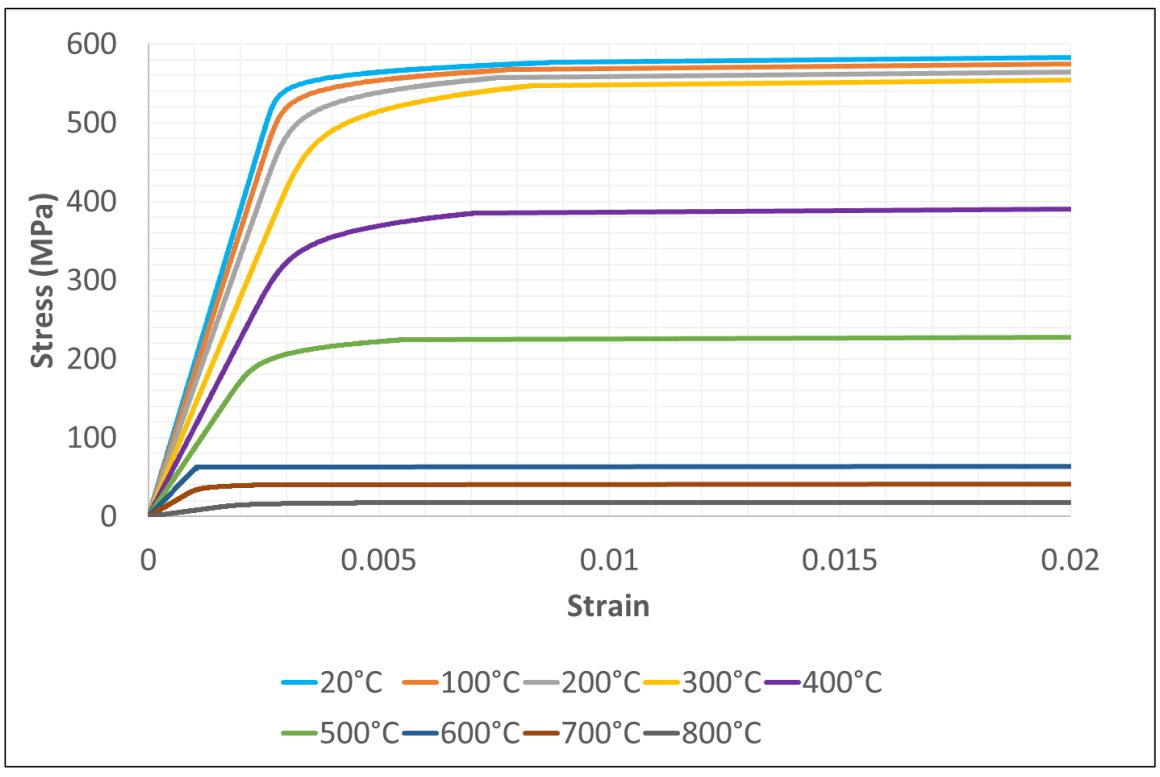

(c) Stress-strain curves of G550 cold-formed steel at elevated temperature used in the FE model

Fig. 14: Stress-strain curves at ambient and elevated temperatures

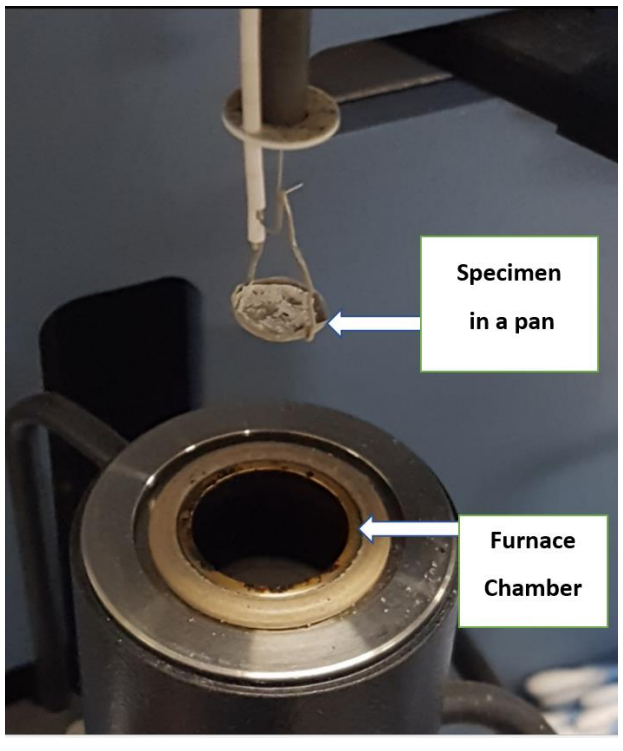

(a) TGA test for obtaining density curve at elevated temperature

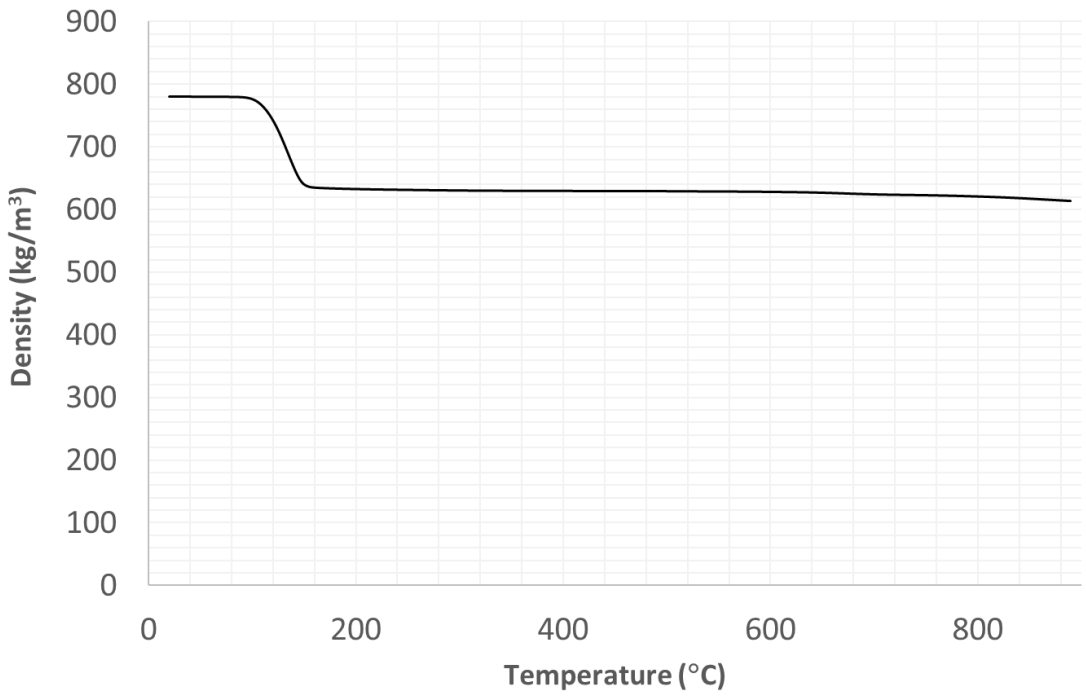

(b) Density curve of gypsum board

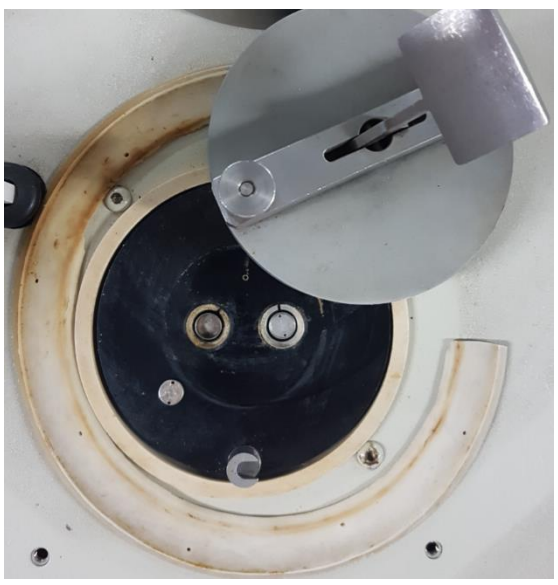

(c) DSC test for specific heat capacity curve of gypsum board

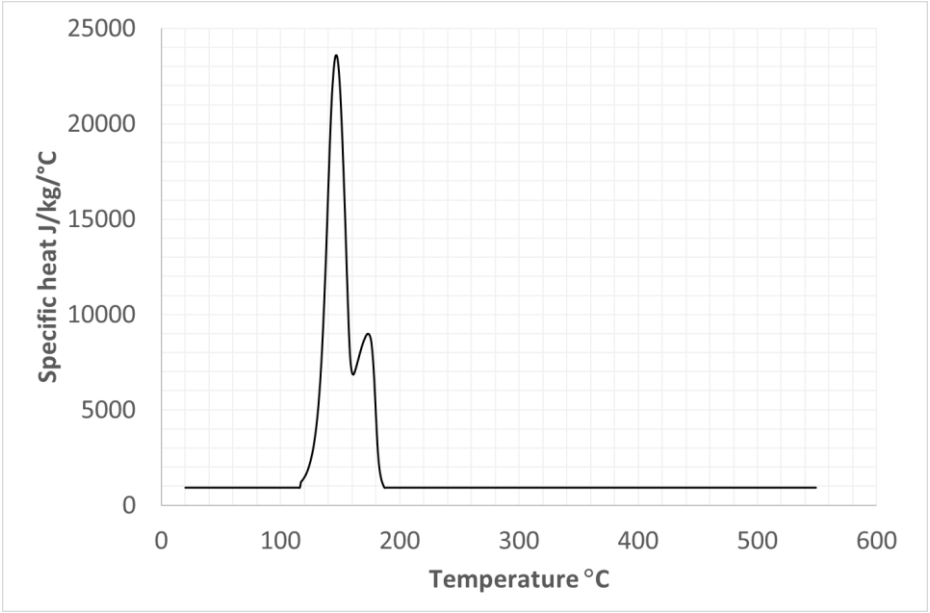

(d) Specific heat capacity curve of gypsum board

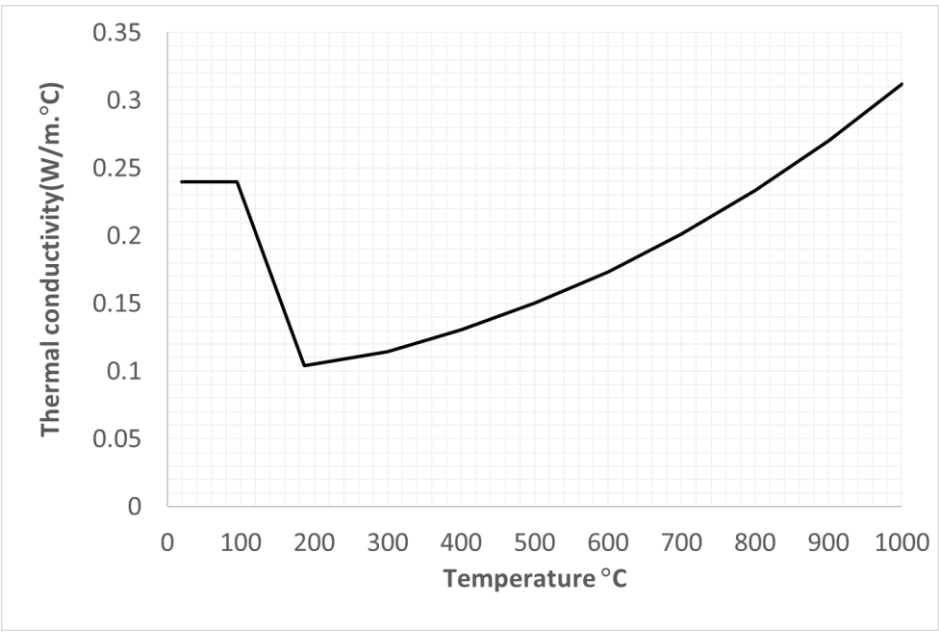

(e) Thermal conductivity curve of gypsum board modified after Rahmanian and Wang [31]

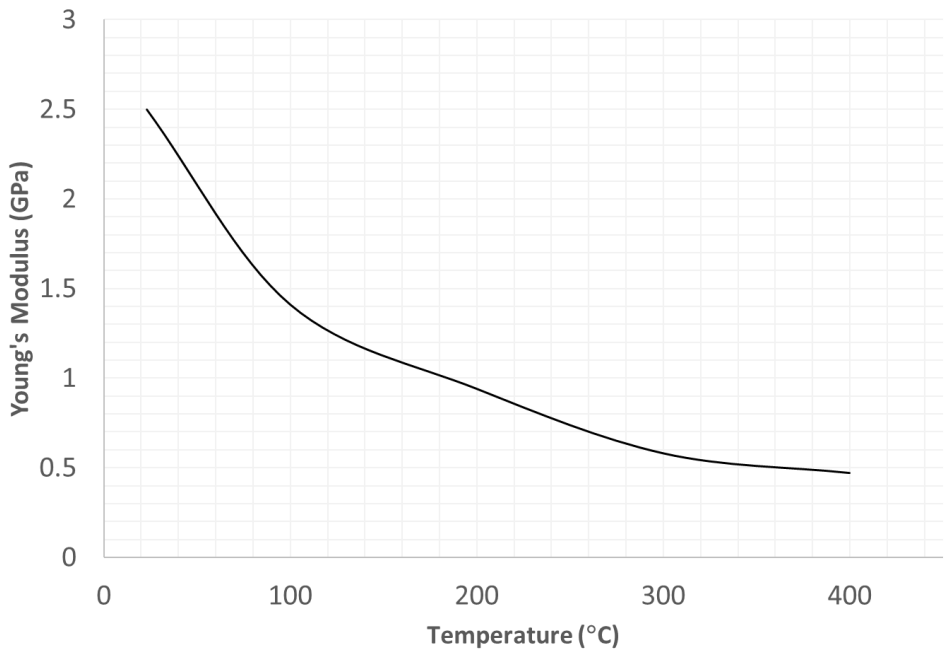

(f) Young’s modulus against temperature graph of gypsum board (Cramer et al. [32])

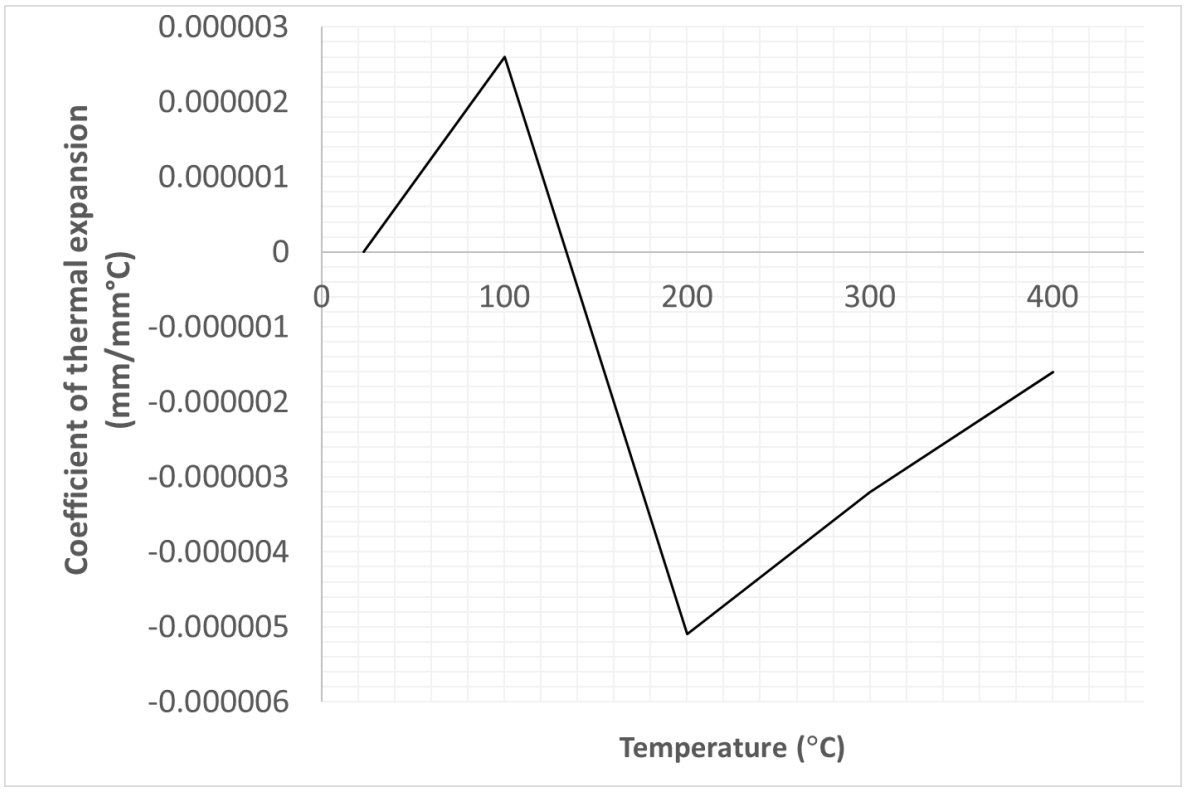

(g) Coefficient of thermal expansion (Cramer et al. [32])

Fig. 15: Thermal properties of the gypsum board used in the FE model

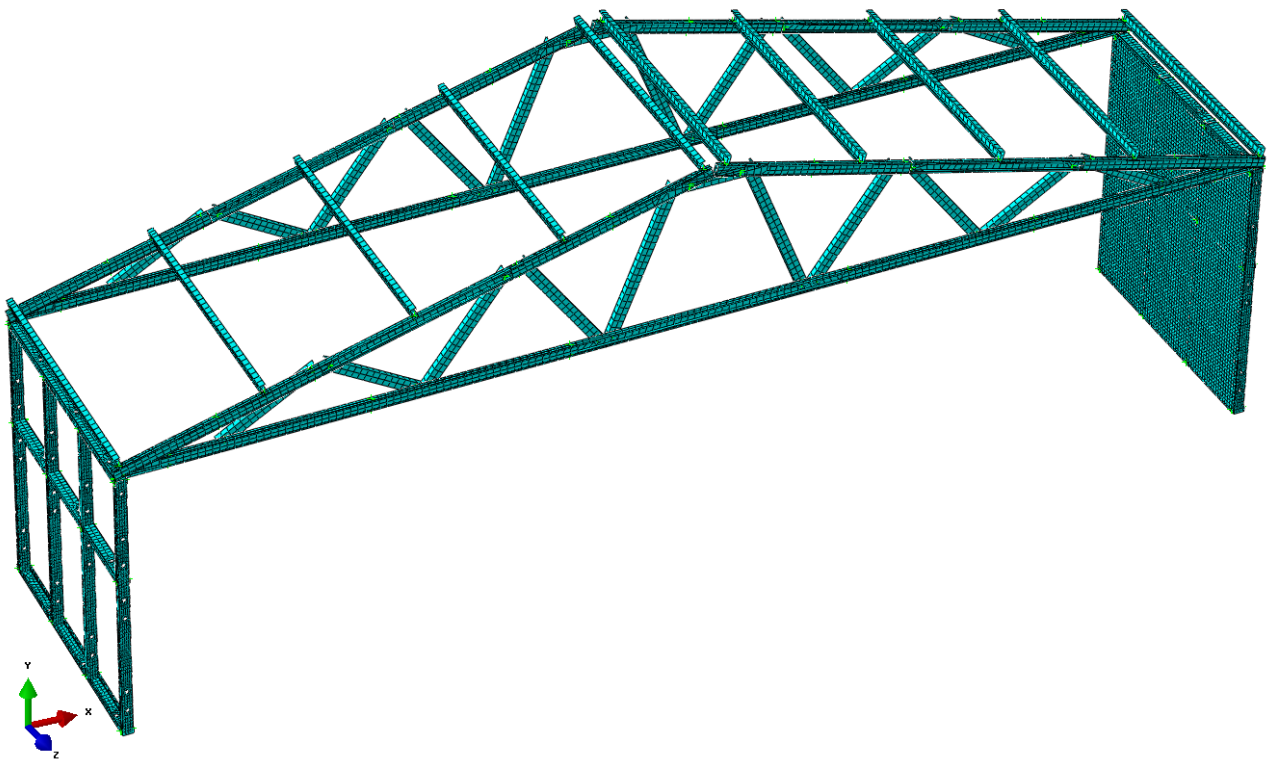

(a) FE meshing

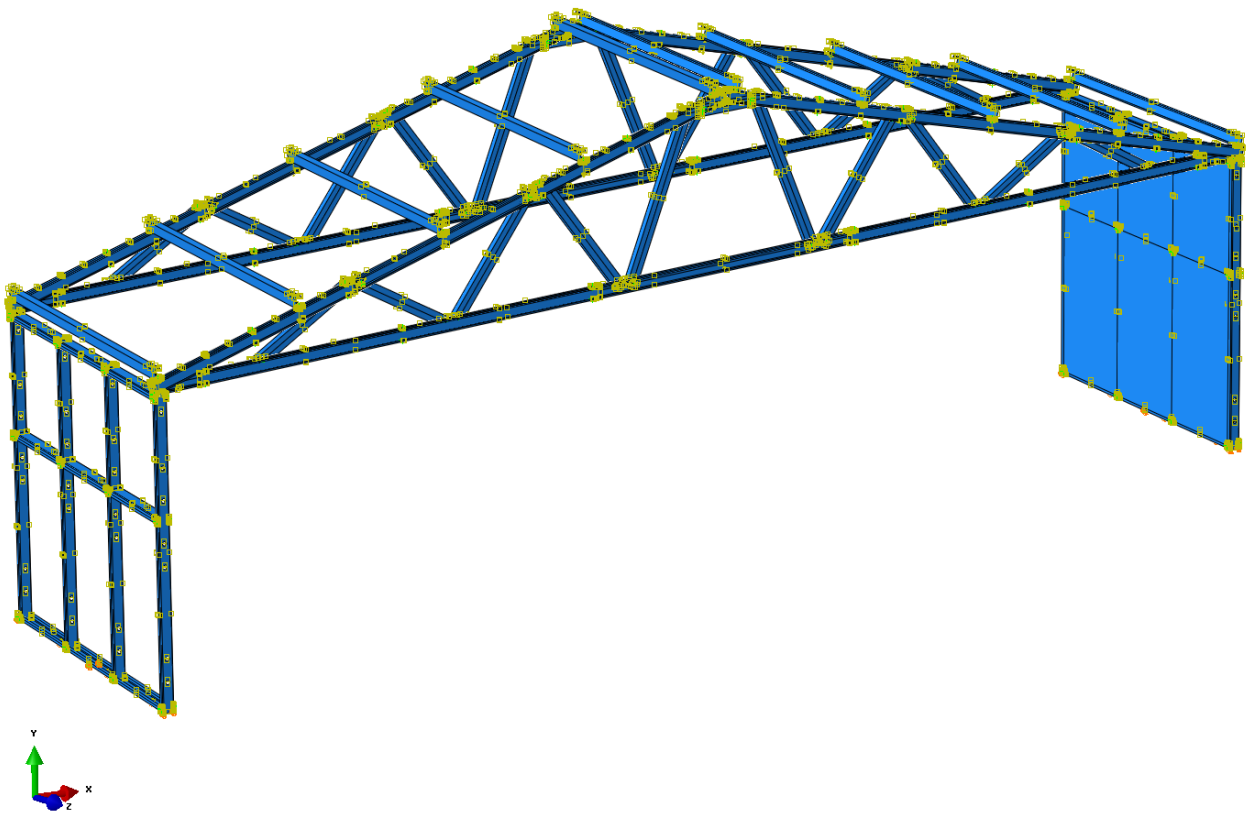

(b) Boundary conditions applied in the FE model

Fig. 16: Details of the FE model for cold-formed steel cantilever wall/truss system

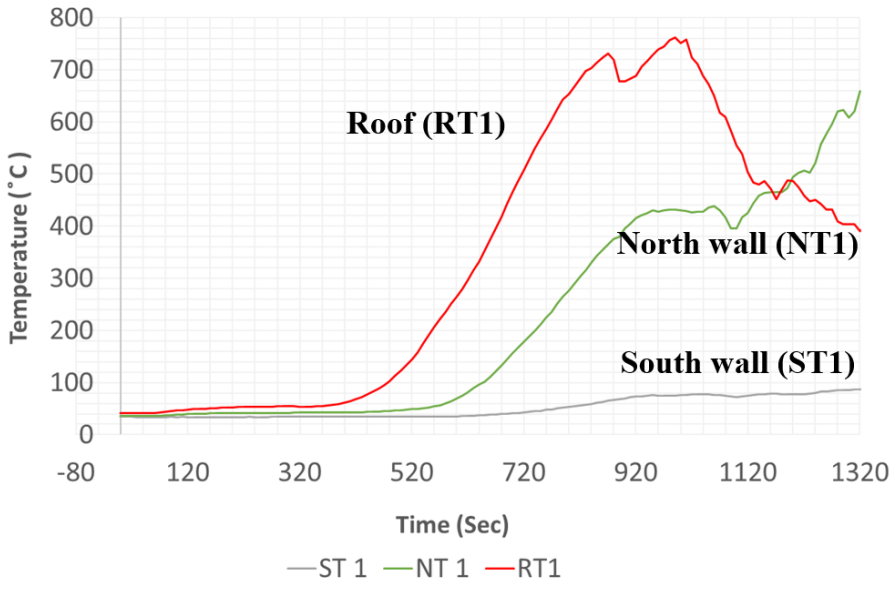

Fig. 17: Temperature against time curves used in FE model

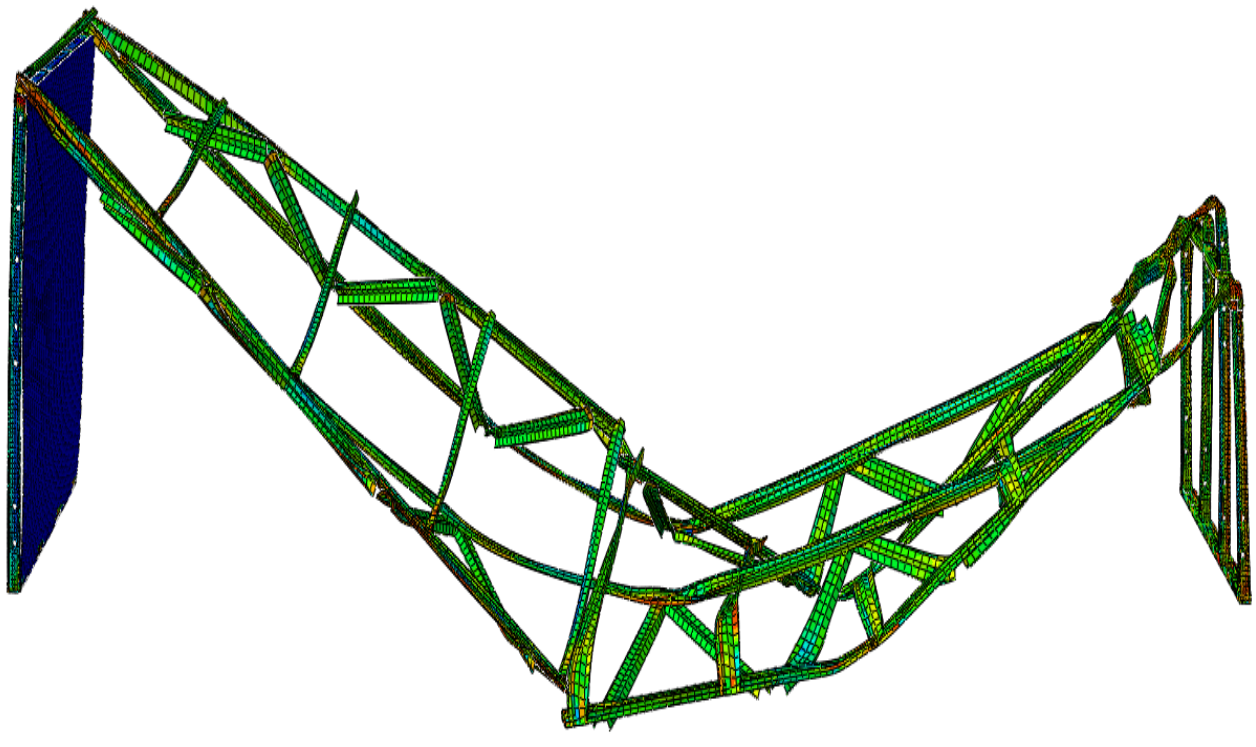

Fig. 18: Final collapse mechanism of FE model

(i) Experimental (ii) FEA

(a) Northern wall

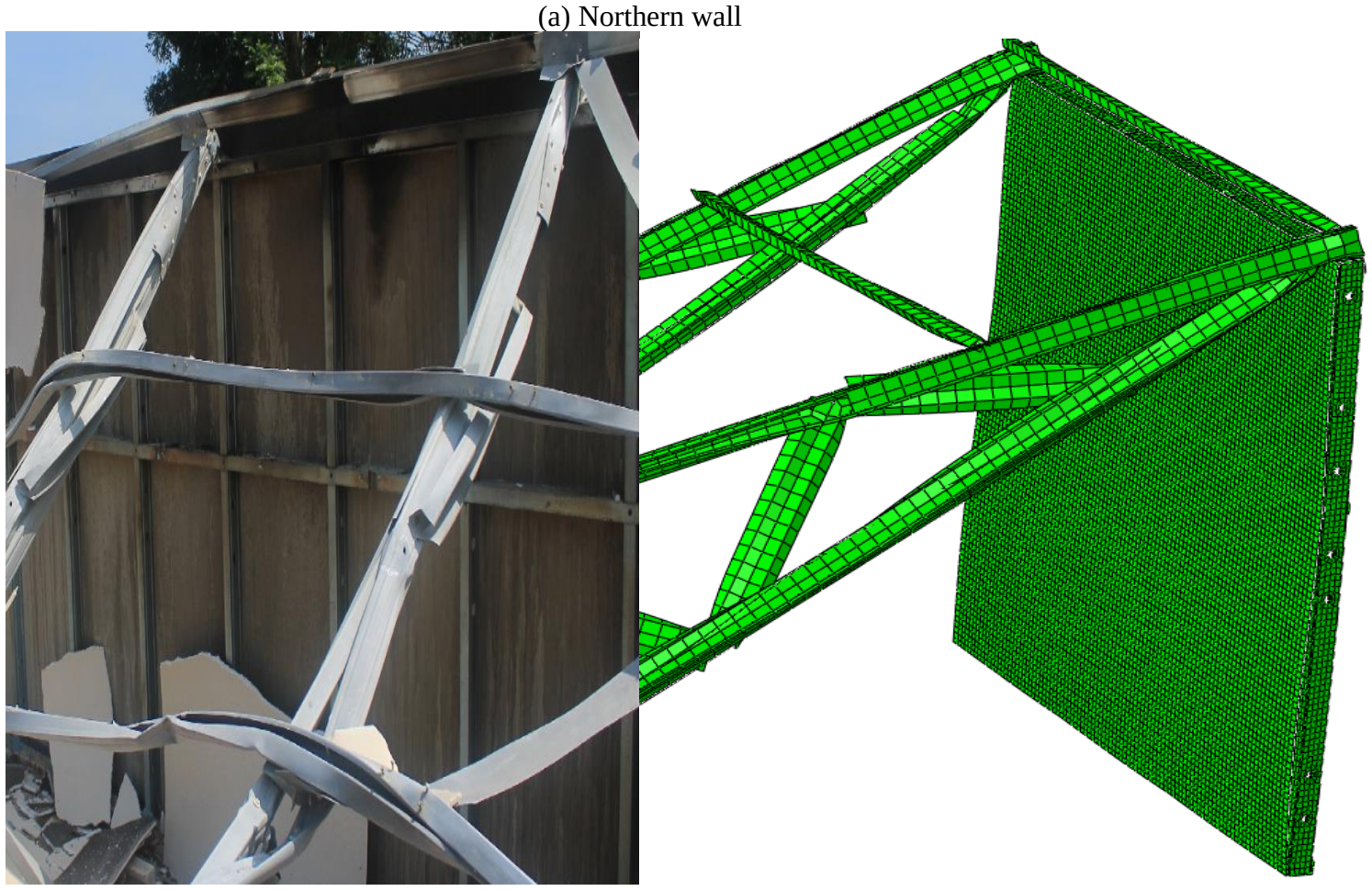

(i) Experimental (ii) FEA

(b) Southern wall

Fig. 19: Comparison of FEA and experimental failure modes

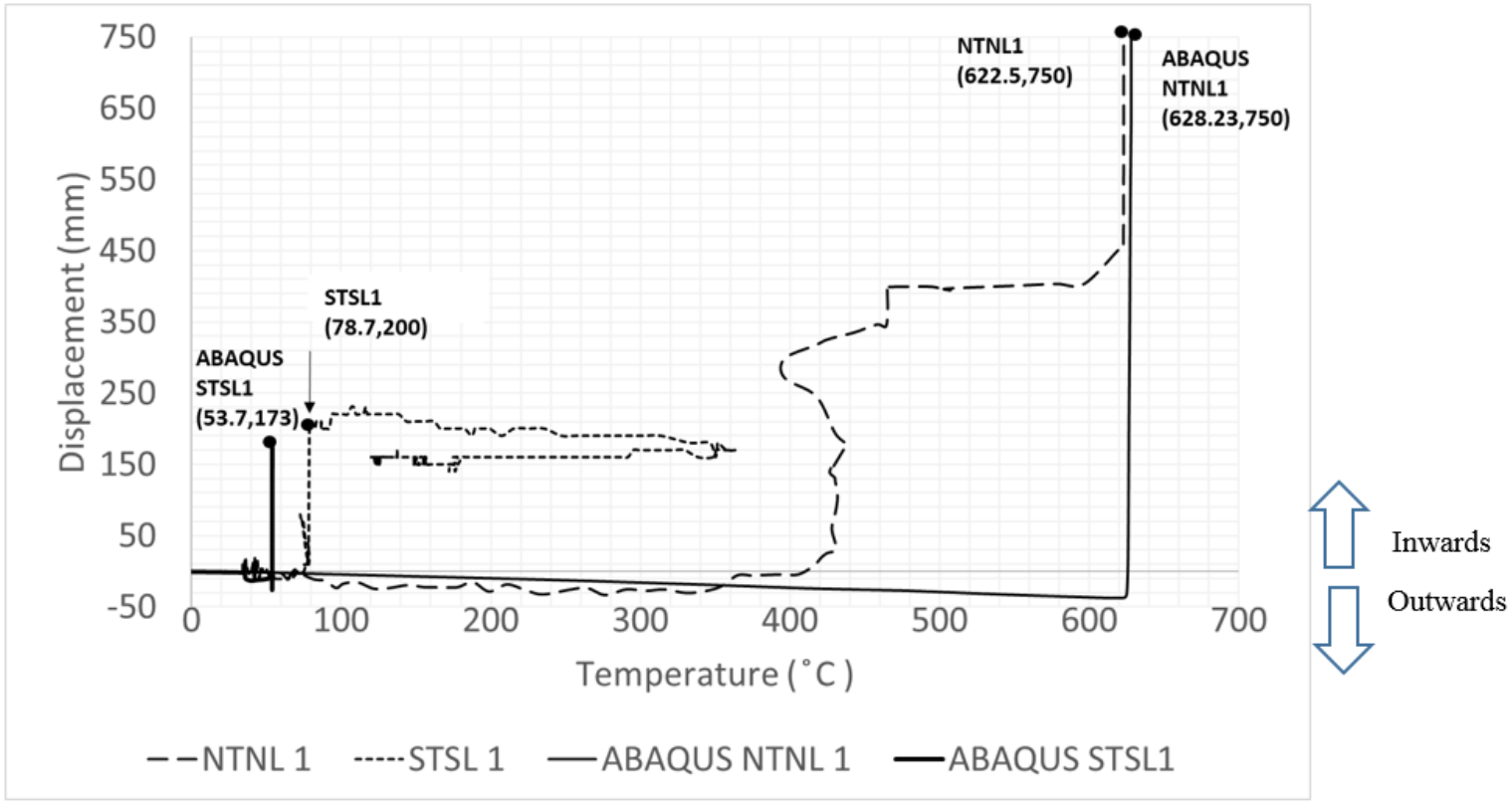

Fig. 20: Horizontal displacement against temperature graph

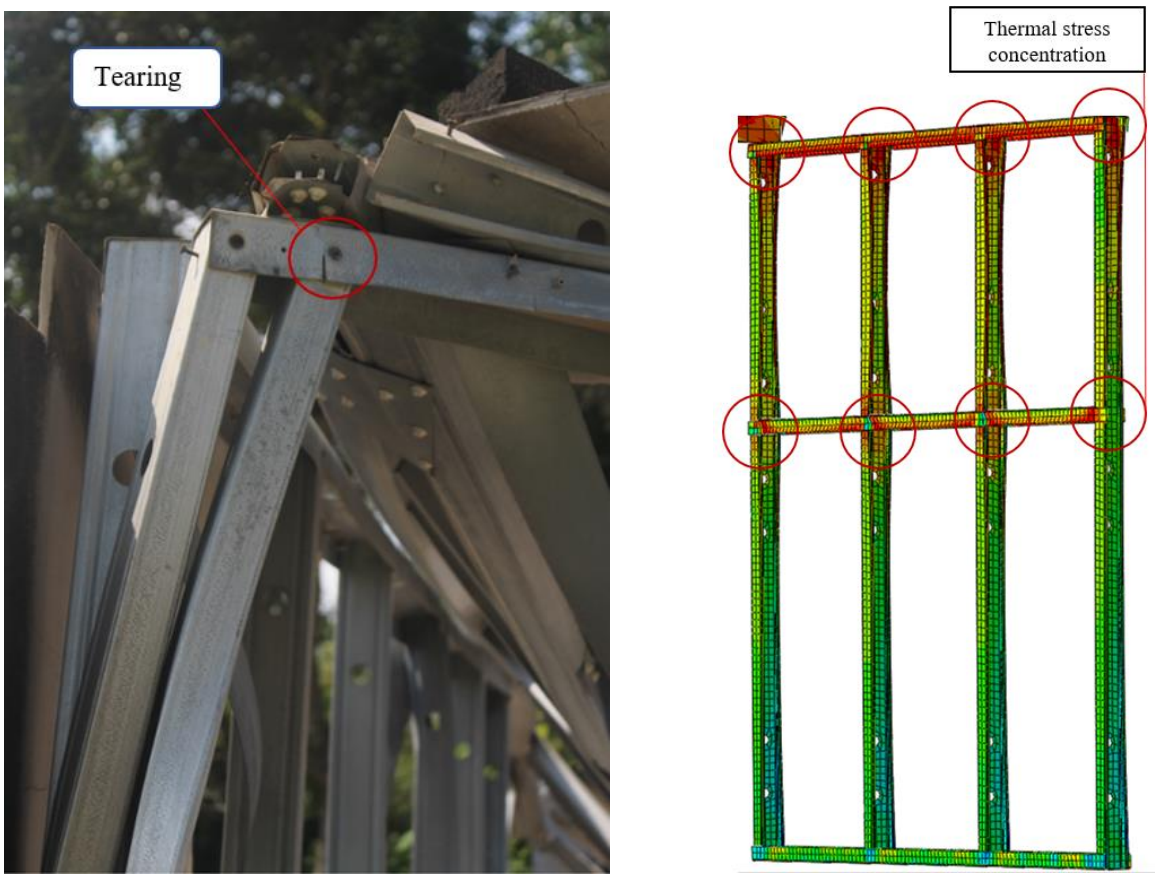

(a) Experimental (Tearing failure) (b) FEA (Thermal stress concentration)

Fig. 21: Tearing failure and thermal stress concentration on the northern wall at 667 sec